

Measurement of the single-top-quark t -channel cross section in pp collisions at $\sqrt{s} = 7$ TeV

The CMS Collaboration*

Abstract

A measurement of the single-top-quark t -channel production cross section in pp collisions at $\sqrt{s} = 7$ TeV with the CMS detector at the LHC is presented. Two different and complementary approaches have been followed. The first approach exploits the distributions of the pseudorapidity of the recoil jet and reconstructed top-quark mass using background estimates determined from control samples in data. The second approach is based on multivariate analysis techniques that probe the compatibility of the candidate events with the signal. Data have been collected for the muon and electron final states, corresponding to integrated luminosities of 1.17 and 1.56 fb⁻¹, respectively. The single-top-quark production cross section in the t -channel is measured to be 67.2 ± 6.1 pb, in agreement with the approximate next-to-next-to-leading-order standard model prediction. Using the standard model electroweak couplings, the CKM matrix element $|V_{tb}|$ is measured to be 1.020 ± 0.046 (meas.) ± 0.017 (theor.).

Submitted to the Journal of High Energy Physics

1 Introduction

Single top quarks can be produced through charged-current electroweak interactions. Due to the large top-quark mass, these processes are well suited to test the predictions of the standard model (SM) of particle physics and to search for new phenomena. Measurements of the single-top-quark production cross section also provide an unbiased determination of the magnitude of the Cabibbo–Kobayashi–Maskawa (CKM) matrix element $|V_{tb}|$.

Single-top-quark production was observed in proton–antiproton collisions at the Tevatron collider with a centre-of-mass energy of 1.96 TeV [1–3]. The cross section increases by a factor of 20 at the Large Hadron Collider (LHC) with respect to the Tevatron. The first measurements of the single-top-quark production cross section in proton–proton collisions at a centre-of-mass energy of 7 TeV were performed by the Compact Muon Solenoid (CMS) [4] and ATLAS [5, 6] experiments.

Previous measurements are compatible with expectations based on approximate next-to-leading-order and next-to-next-to-leading logarithm (NLO+NNLL) perturbative quantum chromodynamics (QCD) calculations. In these calculations, three types of parton scattering processes are considered: t -channel and s -channel processes, and W -associated single-top-quark production (tW). The dominant contribution to the cross section is expected to be from the t -channel process with a cross section of $\sigma_{t\text{-ch.}}^{\text{th.}} = 64.6_{-0.7}^{+2.1} {}_{-1.7}^{+1.5}$ pb [7] for a top-quark mass of $m_t = 172.5$ GeV/ c^2 .

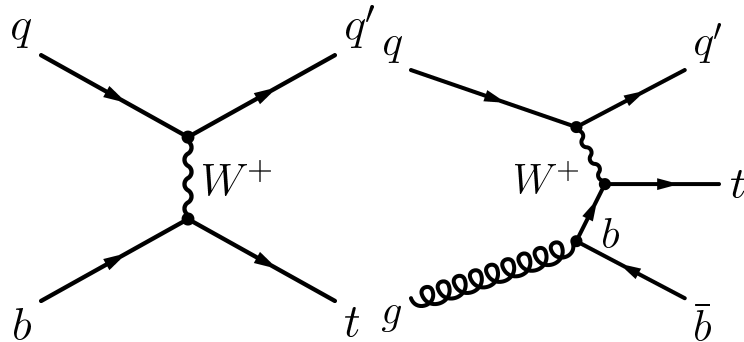


Figure 1: Leading order Feynman diagrams for single-top-quark production in the t -channel: $2 \rightarrow 2$ (left) and $2 \rightarrow 3$ (right).

This paper extends the previous CMS measurement [4] of the t -channel cross section. The single-top-quark production cross section measurement is based on pp collision data at $\sqrt{s} = 7$ TeV collected during 2011 with the CMS experiment, corresponding to integrated luminosities of 1.17 and 1.56 fb^{-1} with muon and electron final states, respectively. Events with leptonically decaying W bosons are selected: $t \rightarrow bW \rightarrow b\ell\nu$ ($\ell = e$ or μ). This measurement is used to determine the CKM matrix element $|V_{tb}|$.

The t -channel event signature (Fig. 1) typically comprises one forward jet scattered off a top quark. The decay products of the top quark mainly appear in the central region of the detector. A dedicated event selection is applied, and then measurements with two complementary approaches are performed. The first approach exploits the reconstructed top-quark mass and one of the angular properties specific to t -channel top-quark production: the forward pseudo-rapidity distribution of the light jet recoiling against the top quark. This analysis is referred to as the $|\eta_j|$ analysis. It is straightforward and robust and has little model dependence. The second approach exploits, via multivariate discriminators, the compatibility of the signal candidates with the event characteristics predicted by the SM for electroweak top-quark production. This approach aims for a precise t -channel cross section measurement by optimising the

discrimination between signal and background. The systematic uncertainties are constrained by simultaneously analysing phase space regions with substantial t -channel single-top-quark contributions and regions where they are negligible. Because of the higher complexity of this approach, two independent multivariate analyses are conducted that cross-check each other. One is based on a Neural Network (NN) and the other on Boosted Decision Trees (BDT). After validating the consistency of the results, the final result is determined by combining the three analyses using the Best Linear Unbiased Estimator (BLUE) [8].

2 CMS Detector

The CMS Detector is described in detail elsewhere [9], and the key components for this analysis are listed below. The main feature of the CMS detector is a superconducting solenoidal magnet with a length of 13 m and a diameter of 6 m which provides an axial magnetic field of 3.8 T. The bore of the solenoid contains various particle detection systems. Charged particle trajectories are recorded by the silicon pixel and strip tracker covering the region $|\eta| < 2.5$, where the pseudorapidity η is defined as $\eta = -\ln[\tan(\theta/2)]$, with θ the polar angle of the trajectory of the particle with respect to the anticlockwise beam direction. A crystal electromagnetic calorimeter (ECAL) and a brass/scintillator hadronic calorimeter (HCAL) surround the tracking volume and extend to $|\eta| < 3.0$. A quartz-fibre and steel absorber Cherenkov-light hadron forward detector extends the calorimeter coverage to $|\eta| < 5.0$. Muons are detected in gas-ionization detectors embedded in the steel return yoke outside the solenoid. The detector is nearly hermetic, which permits good energy balance measurements in the plane transverse to the beam line.

3 Collision Data and Simulation

The present analyses use data sets collected during 2011 corresponding to integrated luminosities of 1.17 and 1.56 fb^{-1} for the muon and electron channels, respectively.

Single-top-quark t -channel signal events from Monte Carlo (MC) simulation used in this study have been generated with the next-to-leading-order (NLO) MC generator POWHEG [10–13] interfaced to PYTHIA 6.4.24 [14] for the parton showering simulation. This ensures good modelling of the $2 \rightarrow 2$ (Fig. 1, left) process and all NLO contributions, in particular of the $2 \rightarrow 3$ diagram (Fig. 1, right). Signal events have also been generated using COMPHEP [15] to study systematic uncertainties related to the MC generator. A top-quark mass of $172.5 \text{ GeV}/c^2$ has been assumed in the simulations.

Several SM processes are taken into account as background to the analysis. The POWHEG generator interfaced with PYTHIA is used to model the single-top-quark tW and s -channel events, which are considered as background in this analysis. The tree-level matrix-element generator MADGRAPH [16] interfaced to PYTHIA is used for top-quark pair ($t\bar{t}$) production and for inclusive single boson production $V + X$, where $V = W$ or Z , and X can indicate one or more light or heavy partons. In the following, we will explicitly distinguish the processes with V +light partons, Wc , and VQQ , with $Q = b$ or c . A procedure implemented during the event generation and based on the “MLM prescription” [17] avoids double counting between matrix element and parton shower generated jets. The remaining background samples are simulated using PYTHIA. These include diboson production (WW, WZ, ZZ), γ +jets, and multijet QCD enriched events with electrons or muons coming from the decays of b and c quarks, as well as muons from the decay of long-lived hadrons. The CTEQ6 [18] parton distribution functions are used for all simulated samples.

All generated events undergo a full simulation of the detector response according to the CMS implementation of GEANT4 [19], and are processed by the same reconstruction software used for collision data.

4 Event Selection and Reconstruction

Events are characterized by a single isolated muon or electron and momentum imbalance due to the presence of a neutrino, with one central b jet from the top-quark decay. An additional light-quark jet from the hard-scattering process is often present in the forward direction. A second b jet produced in association with the top quark can also be present (Fig. 1, right), although it yields a softer p_T spectrum with respect to the b jet coming from the top-quark decay.

The trigger used for the online selection of the analysed data for the muon channel is based on the presence of at least one isolated muon with a transverse momentum $p_T > 17 \text{ GeV}/c$. For the electron channel, an isolated electron trigger with a transverse momentum $p_T > 27 \text{ GeV}/c$ was used for the initial data-taking period, corresponding to an integrated luminosity of 216 pb^{-1} . For the remaining data-taking period, a trigger selecting at least one electron with $p_T > 25 \text{ GeV}/c$ and a jet with $p_T > 30 \text{ GeV}/c$ was used. The jet is identified in the trigger processing as coming from a fragmentation of a b quark using the Track Counting High-Efficiency (TCHE) b-tagging algorithm described in Ref. [20].

At least one primary vertex is required, reconstructed from a minimum of four tracks, with a longitudinal distance of less than 24 cm, and a radial distance of less than 2 cm from the nominal interaction point. To select good muon and electron candidates, the same lepton identification as described in Ref. [21] is applied. Electrons, muons, photons, and charged and neutral hadron candidates are reconstructed and identified using the CMS particle-flow (PF) algorithm [22]. The missing transverse momentum vector $\vec{\cancel{p}}_T$ is reconstructed from the momentum imbalance of PF particle candidates in the plane transverse to the beams direction. The magnitude of $\vec{\cancel{p}}_T$ is the missing transverse energy E_T . The presence of exactly one isolated muon or electron candidate originating from the primary vertex is required in the event. Muon candidates are selected by requiring a transverse momentum $p_T > 20 \text{ GeV}/c$ and a pseudorapidity $|\eta| < 2.1$. Electron candidates must have a transverse momentum $p_T > 30 \text{ GeV}/c$ and $|\eta| < 2.5$. Lepton isolation I_{rel}^ℓ is defined as the sum of the transverse energy deposited by stable charged hadrons, neutral hadrons, and photons in a cone of $\Delta R = \sqrt{(\Delta\eta)^2 + (\Delta\phi)^2} = 0.4$ around the charged-lepton track, divided by the transverse momentum of the lepton. Muon isolation is ensured by requiring $I_{\text{rel}}^\ell < 0.15$, while the isolation requirement is tightened to 0.125 for electrons. An electron candidate is rejected if it is identified as originating from the conversion of a photon into an electron–positron pair or if it fails the identification criteria described in Ref. [21]. Events are also rejected if an additional muon candidate is present that passes looser quality criteria, namely, $p_T > 10 \text{ GeV}/c$, $|\eta| < 2.5$, and $I_{\text{rel}}^\ell < 0.2$. For additional electrons, the required transverse momentum is $p_T > 15 \text{ GeV}/c$.

Jets are defined by clustering PF candidates according to the anti- k_T algorithm [23] with a distance parameter of 0.5. The analysis considers jets whose calibrated transverse momentum is greater than $30 \text{ GeV}/c$ for $|\eta| < 4.5$. An event is accepted for further analysis only if at least two such jets are reconstructed. A jet is identified as coming from a b-quark fragmentation if it passes a tight threshold on the Track Counting High-Purity (TCHP) b-tagging algorithm [20] corresponding to a misidentification probability of 0.1%. The difference between simulated and measured b-tagging efficiencies, for true and misidentified b jets, is corrected by scaling

the simulated event yields according to p_T -dependent scale factors determined from control samples from the data [20].

Events with a muon that is not from a leptonic decay of a W boson are suppressed by requiring a reconstructed transverse W boson mass $m_T = \sqrt{2p_T \cancel{E}_T (1 - \cos(\Delta\phi_{\ell, \vec{p}_T}))} > 40 \text{ GeV}/c^2$, where $\Delta\phi_{\ell, \vec{p}_T}$ is the azimuthal angle between the muon and the \vec{p}_T directions and p_T is the transverse momentum of the muon. For the electron channel, where the QCD multijet contamination is larger, the requirement $\cancel{E}_T > 35 \text{ GeV}$ is applied instead of the m_T selection.

To classify signal and control samples, different event categories are defined and denoted as “ n -jets m -btags”, where n is the number of selected jets (2, 3, or 4) and m is the number of selected b-tagged jets (0, 1, or ≥ 2). The single-top-quark t -channel signal is primarily contained in the category “2-jets 1-btag”, followed by “3-jets 1-btag”, as the second b jet, which is produced in association with the top quark, is mostly out of acceptance. The other categories are dominated by background processes with different compositions. In particular, the “2/3-jets 0-btags” categories are enriched in events with a W boson produced in association with light partons (u, d, s, g). The “3-jets 2-btags” and “4-jets 0/1/2-btags” categories are enriched in $t\bar{t}$ events.

To extract the signal content, the NN and BDT analyses utilize the following six categories simultaneously for the measurement of the signal cross section: “2-jets 1-btag”, “3-jets 1-btag”, “4-jets 1-btag”, “2-jets 2-btags”, “3-jets 2-btags”, and “4-jets 2-btags”. The latter four categories are used to constrain nuisance parameters (e.g. the b-tagging efficiency or background normalisation). Besides these six categories, the three 0-tag categories are used to check the modelling of input variables. The $|\eta_j|$ analysis extracts the signal content from the “2-jets 1-btag” category only, but uses the “2-jets 0-btags” and “3-jets 2-btags” categories to check the modelling of backgrounds.

The reconstruction of the top quark from its decay products leads to multiple choices of possible top-quark candidates. In the first step, the W-boson candidate is reconstructed from the charged lepton and from \vec{p}_T following the procedure described in Ref. [4]. In the second step, the top-quark candidate is reconstructed by combining the W-boson candidate with a jet identified as coming from a b quark, and its mass $m_{\ell\nu b}$ is calculated. Depending on the analysis category, the ambiguity in the choice of the b-quark jet from the top-quark decay and the recoiling light quark has to be resolved. Events in the “2-jets 1-btag” category have no ambiguity: the b-tagged jet is associated with the top-quark decay, and the other jet is considered to be a light-quark jet.

In the other categories, the top quark and light-quark jet reconstruction has been optimized for the purpose of each analysis and differs among them. In the NN and BDT analyses, the most forward jet is chosen to be the light-quark jet in categories where two jets and zero or two b tags are required. The other jet is associated with the top-quark decay. In categories where three or more jets are required, in the case of one or two required b tags, the jet with the lowest value of the TCHP discriminator is assumed to originate from the light quark. If no b tag is required, the most forward jet is associated with the light quark. From the remaining jets, the one which together with the reconstructed W boson has a reconstructed top-quark mass $m_{\ell\nu b}$ closest to $m_t = 172.5 \text{ GeV}/c^2$ is chosen as the b jet coming from the top-quark decay. In the $|\eta_j|$ analysis, the jet with the highest value of the TCHP discriminator is used for the top-quark reconstruction in the “2-jets 0-btags” and “3-jets 2-btags” categories. The inclusive $|\eta|$ distribution of both jets is used in “2-jets 0-btags”, while for the “3-jets 2-btags” category the $|\eta|$ of the non-b-tagged jet is used.

In the $|\eta_{j'}|$ analysis the invariant mass $m_{\ell\nu b}$ of the reconstructed top quark is used to further divide the “2-jets 1-btag” category into a t -channel enriched signal region (SR), defined by selecting events within the mass range $130 < m_{\ell\nu b} < 220 \text{ GeV}/c^2$, and a W boson and $t\bar{t}$ enriched sideband region (SB), defined by selecting events that are outside this $m_{\ell\nu b}$ mass window. The event yield in the SR is summarised in Table 1 for the muon and electron channels, together with expectations from simulated signal and backgrounds, and for QCD multijet events, which are determined from control samples of data, as described in Section 5.1.

Table 1: Event yield with statistical uncertainties of the $|\eta_{j'}|$ analysis for the signal and main background processes in the signal region, after applying the $m_{\ell\nu b}$ mass requirement for the μ and e channels. The yields are taken from simulation except for the QCD multijet yield, which is obtained from control samples of data as described in Section 5.1. The normalisation of the $Wc(\bar{c})$ and $Wb(\bar{b})$ processes is further discussed in Section 5.2.

Process	Muon yield	Electron yield
t -channel	617 ± 3	337 ± 2
tW channel	107 ± 1	70.2 ± 0.9
s -channel	25.6 ± 0.5	14.7 ± 0.4
$t\bar{t}$	661 ± 6	484 ± 5
W + light partons	92 ± 7	38 ± 4
$Wc(\bar{c})$	432 ± 14	201 ± 9
$Wb(\bar{b})$	504 ± 14	236 ± 10
Z + jets	87 ± 3	13 ± 1
Dibosons	23.3 ± 0.4	10.7 ± 0.3
QCD multijet	77 ± 3	62 ± 3
Total	2626 ± 22	1468 ± 16
Data	3076	1588

5 Background Estimation and Control Samples

Several control data samples are used for two main purposes:

- to check the distributions of variables used as inputs to the analyses and the agreement between data and simulation;
- to determine from data the yields and distributions of variables of interest for the main background processes.

All the analyses use rate and shape determinations from QCD multijet background data. The $|\eta_{j'}|$ analysis also determines the yields and distributions of the background processes by using W boson production in association with jets from light quarks as well as c and b quarks. The NN and BDT analyses take the shape of the W+jets background from MC simulation, but consider the impact of shape uncertainties in the evaluation of the systematic uncertainties. In all three analyses the rate of the W+jets background is determined “in situ” by the signal extraction method as described in Section 9.

5.1 QCD Multijet Background Estimation

The yield of the QCD multijet background in the different categories is measured by performing fits to the distributions of the transverse W boson mass m_T in the muon channel and E_T in

the electron channel. A maximum-likelihood fit to the distribution of m_T or \cancel{E}_T is performed assuming the following parameterisation: $F(x) = a \cdot S(x) + b \cdot B(x)$, where x is m_T or \cancel{E}_T for the muon and electron channels, respectively, and $S(x)$ and $B(x)$ are the expected distributions for the sum of all processes including a W boson in the final state and for QCD multijet events, respectively. The function $S(x)$ is taken from simulation, while $B(x)$ is extracted directly from data. The parameters a and b are determined from the fit. The QCD multijet background yield is estimated to be the area of the fitted curve $b \cdot B(x)$ in the range $m_T > 40 \text{ GeV}/c^2$ for the muon channel and $\cancel{E}_T > 35 \text{ GeV}$ for the electron channel, as mentioned in Section 4.

QCD multijet enriched samples from data are used to model the distributions $B(x)$ of m_T and \cancel{E}_T . For the muon channel, this sample is selected by inverting the isolation requirement. For the electron channel, the selected electron is required to fail at least two of the three following quality requirements: $I_{\text{rel}}^\ell < 0.1$, the distance of closest approach to the primary vertex on the x - y plane $\delta_{xy} < 0.02 \text{ cm}$, and the electron identification criteria given in Ref. [21]. It was verified by simulation that the m_T and \cancel{E}_T distributions for QCD multijet like events are not significantly affected by this altered event selection.

In the $|\eta_{j'}|$ analysis the fits to the m_T and \cancel{E}_T distributions cannot be performed reliably in the SR and SB separately due to the limited size of the simulated samples, which would introduce large uncertainties in the signal modelling. For this reason, the fit is performed on the entire “2-jets 1-btag” sample. The number of QCD multijet events in the SB and SR regions is determined by scaling the total QCD multijet yield, obtained from the fit, by the fraction of events in the two regions (SB and SR) of the $m_{\ell\nu b}$ distribution, as determined from the QCD multijet enriched region. In the simulation, the distributions of the relevant variables obtained from the QCD multijet enriched sample are consistent with the ones in the SR. The QCD multijet yields restricted to the SR are reported in Table 1.

For all three analyses, the relative uncertainties on the QCD multijet yield estimates are taken to be $\pm 50\%$ for the muon channel and $\pm 100\%$ for the electron channel. Several cross checks have been performed; for example, the same fits have been repeated taking $B(x)$ from simulation for both channels. Moreover, the choice of $x = m_T$ or \cancel{E}_T has been inverted for the muon and electron channels, in this way performing fits on m_T for the electron channel and \cancel{E}_T for the muon channel. The results in each case are in agreement with the previous estimate within the assumed uncertainties.

5.2 W+jets Background Estimation and Other Control Samples

A check of the modelling for the W+jets background is carried out for each of the three analyses in the 0-tag control regions. In particular, the “2-jets 0-btags” category is highly enriched in W+light jet events. The modelling of $t\bar{t}$ background is checked in the “3-jets 2-btags” as well as the “4-jets” categories. In general, the event yields are reasonably well reproduced by the simulation within the systematic uncertainties. The shapes of the relevant variables, $|\eta_{j'}|$ and $m_{\ell\nu b}$, and the input variables of the NN and BDT analyses show good agreement between data and simulation.

Table 1 shows a difference between the total observed and expected yields for the $|\eta_{j'}|$ analysis. This difference can be attributed to excesses in data for the Wb+X and Wc+X processes. The ATLAS collaboration reported in Ref. [24] that the fiducial W+b-jet cross section in the lepton and one or two jets final state is a factor of 2.1 larger than the NLO prediction, but is still consistent at the level of 1.5 standard deviations with this SM prediction.

Motivated by these observed excesses in comparison to the SM NLO calculations, the $|\eta_{j'}|$ anal-

ysis determines the W +jets background yield and $|\eta_{j'}$ distribution from data. The $|\eta_{j'}$ distribution for W +jets process is extracted from the SB by subtracting the $|\eta_{j'}$ distribution of all other processes from the data. The event yield and $|\eta_{j'}$ distributions used for these subtractions are taken from simulations of $t\bar{t}$, single-top-quark s - and tW - channels, and diboson production. The QCD multijet event yield and $|\eta_{j'}$ distribution are extracted from data and extrapolated to the SB as described in Section 5.1. The $|\eta_{j'}$ distribution for W +jets processes in the SB is therefore used in the SR for the signal extraction procedure (see Section 6), assuming that the shapes in the SB and SR are compatible with each other. For the muon channel, the compatibility of the distributions in the two regions has been verified through a Kolmogorov–Smirnov compatibility test, yielding a p -value of 0.47, and a χ^2 test, yielding a p -value of 0.63. For the electron channel, the Kolmogorov–Smirnov compatibility test has a p -value of 0.51 and the χ^2 test a p -value of 0.60. The stability of the extracted shape has been tested by varying the sample composition in terms of $t\bar{t}$ and signal fractions by 20% and 100%, respectively. The extracted shapes are compatible with a p -value greater than 0.9 in both cases.

6 The $|\eta_{j'}$ Analysis

The signal yield is extracted using a maximum-likelihood fit to the observed distribution of $|\eta_{j'}$. The signal distribution for the fit is taken from simulation. The W/Z +jets component of the background is normalised to the value obtained from the extraction procedure described in Section 5.2, and then added to the diboson processes, resulting in the electroweak component of the background for the fit. The signal and the electroweak components are unconstrained in the fit, whereas the QCD multijet component is fixed to the result determined in Section 5.1. A Gaussian constraint is applied to $t\bar{t}$ and other top-quark backgrounds. Figure 2 shows the distribution of $|\eta_{j'}$ obtained from the fit. Figure 3 shows the distribution of the reconstructed

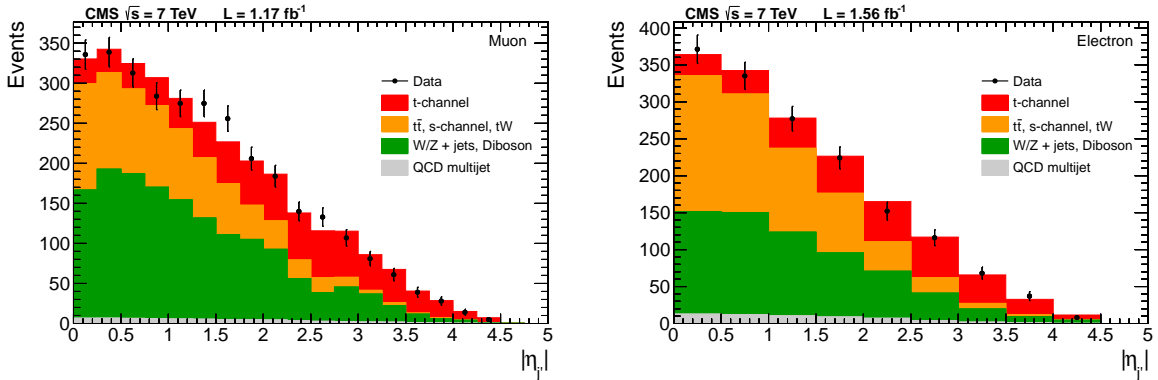


Figure 2: Result of a simultaneous fit to $|\eta_{j'}$ in the muon (left) and electron (right) decay channels.

top-quark mass $m_{\ell\nu b}$ normalised to the fit results, restricting to the highly enriched region of single-top-quark events for $|\eta_{j'}| > 2.8$.

Single-top-quark t -channel production at the LHC is expected to be characterised by two features. First, the top-quark cross section is about a factor two larger than the top-anti-quark cross section [7]. This can be experimentally accessed via the charge of the muon or electron. Second, top quarks are almost 100% polarised with respect to a certain spin axis due to the $V-A$ nature of the couplings. This can be studied via the $\cos\theta^*$ distribution [25], where θ^* is defined as the angle between the charged lepton and the non- b -tagged jet, in the reconstructed top-quark rest

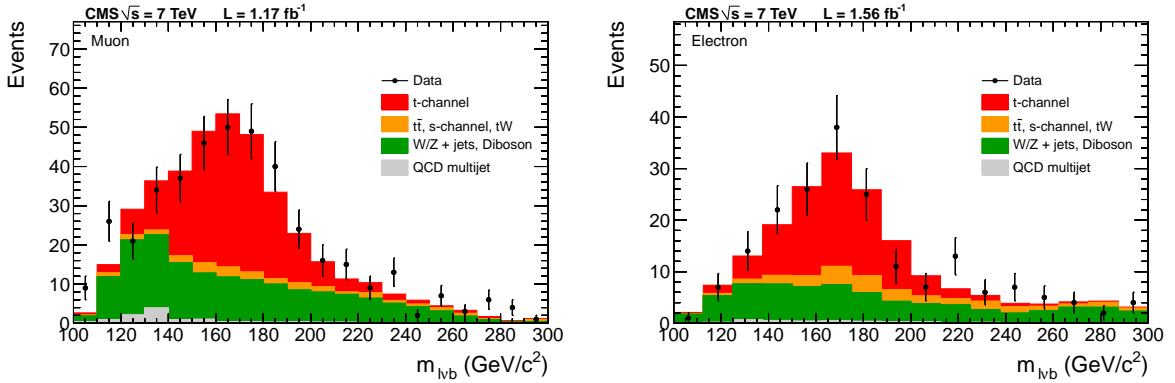


Figure 3: Distributions of $m_{\ell\nu_b}$ requiring $|\eta_{j'}| > 2.8$, for muons (left) and electrons (right), obtained by normalising each process yield to the value from the fit. Because of limited simulated data, the background distribution is smoothed by using a simple spline curve.

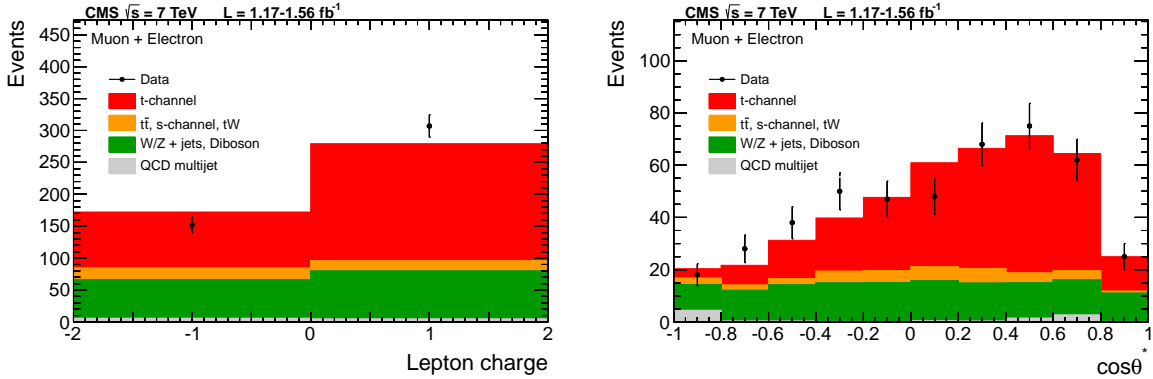


Figure 4: Distinct single-top-quark t -channel features in the SR for $|\eta_{j'}| > 2.8$, for the electron and muon final states combined. The charge of the lepton (left) and $\cos \theta^*$ (right). All processes are normalised to the fit results. Because of limited simulated data, the background distribution is smoothed by using a simple spline curve (right).

frame. The observed charge asymmetry and the $\cos \theta^*$ distribution are presented in Fig. 4 for muon plus electron events in the SR, for $|\eta_{j'}| > 2.8$.

7 Neural Network Analysis

In the NN analysis, several kinematic variables, which are characteristic of SM single-top-quark production, are combined into a single discriminant by applying an NN technique. The NEUROBAYES package [26, 27] used for this NN analysis combines a three-layer feed-forward NN with a complex, but robust, preprocessing. To reduce the influence of long tails in distributions, input variables are transformed to be Gaussian distributed. In addition, a diagonalisation and rotation transformation is performed such that the covariance matrix of the transformed variables becomes a unit matrix. To obtain good performance and to avoid overtraining, the NN uses Bayesian regularisation techniques for the training process. The network input layer consists of one input node for each input variable plus one bias node. The hidden layer is adapted to this particular analysis and consists of one more node than the input layer. The output node gives a continuous discriminator output in the interval $[-1, 1]$. For the training of the NN,

after applying the full event selection as described in Section 4, simulated samples of signal t -channel single-top-quark events and background events from $t\bar{t}$, W +jets, and Z +jets samples are used. The ratio of signal to background events in the training is chosen to be 50:50 and the background processes are weighted according to the SM prediction, as outlined in Section 5. The NN is trained such that t -channel single-top-quark events tend to have discriminator values close to 1, while background events tend to have discriminator values near -1 . Because of their different event selections, separate neural networks are trained for muon and electron events.

During the preprocessing, the training variables are ranked by the significance of their correlation to the target discriminator output. The correlation matrix of all training variables and the target value is calculated. The variable with the smallest correlation to the target is removed and the loss of correlation is calculated. This is repeated until the correlation of all variables with the target is determined. The significance of a variable is calculated by dividing the loss of correlation with the target by the square root of the sample size. In order to select variables which contain information that is not already incorporated by other variables, a selection criterion of $\geq 3\sigma$ on the significance has been chosen. A set of 37 variables remains for the muon channel when applying this selection criterion. For the electron channel, a set of 38 variables remains. The validity of the description of these input variables and the output of the NN discriminant is confirmed in data with negligible signal contribution. Furthermore, it is verified with a bootstrapping technique [28] that the bias of the cross section measurement due to a possible overtraining of the NN is negligible.

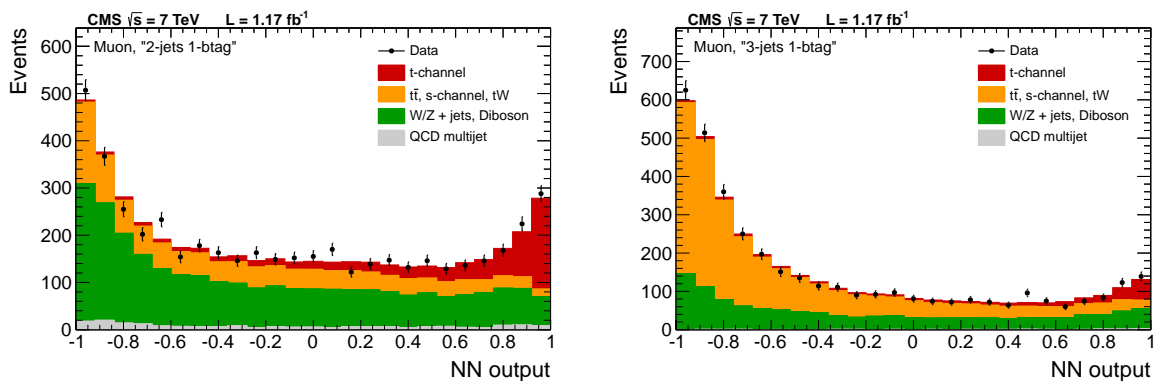


Figure 5: Distributions of the NN discriminator output in the muon channel for the “2-jets 1-btag” (left) and “3-jets 1-btag” (right) categories. Simulated signal and background contributions are scaled to the best fit results.

The variables with the highest ranking in both networks are $|\eta_j|$, m_T , the invariant mass of the two leading jets, and the total transverse energy of the event.

The distributions of the NN discriminator in the “2-jets 1-btag” and “3-jets 1-btag” signal categories are shown in Fig. 5 for the muon channel and in Fig. 6 for the electron channel. For the remaining categories “2-jets 2-btags”, “3-jets 2-btags”, “4-jets 1-btag”, and “4-jets 2-btags”, the events are combined into one plot in Fig. 7 for the muon channel on the left and for the electron channel on the right.

8 Boosted Decision Trees Method

The BDT method was previously used in the first CMS measurement of the t -channel cross section [4]. The current analysis uses a significantly larger data sample. It has been optimised

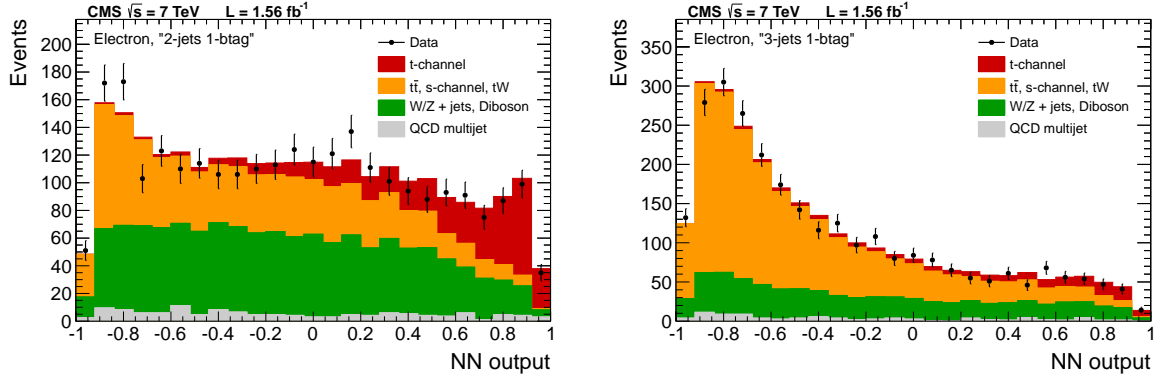


Figure 6: Distributions of the NN discriminator output in the electron channel for the “2-jets 1-btag” (left) and “3-jets 1-btag” (right) categories. Simulated signal and background contributions are scaled to the best fit results.

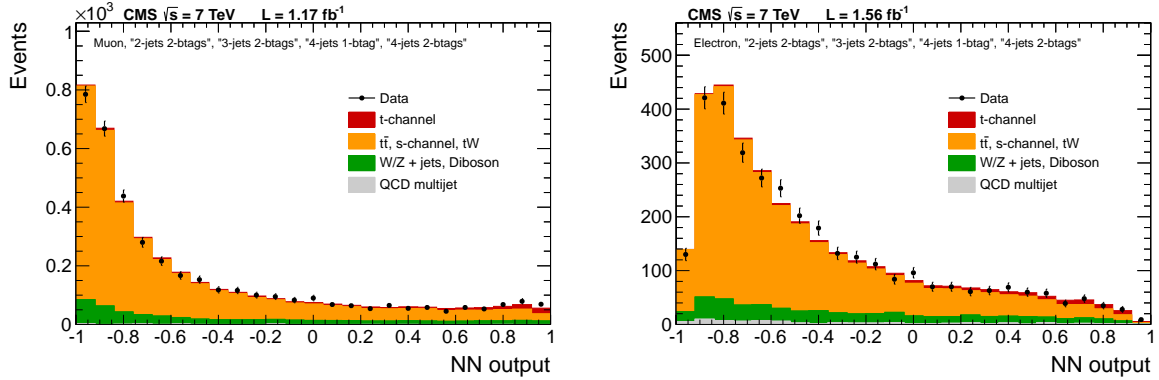


Figure 7: Distributions of the NN discriminator output in the background dominated region. All events from the signal depleted categories “2-jets 2-btags”, “3-jets 2-btags”, “4-jets 1-btag”, and “4-jets 2-btags” are combined for the muon channel (left) and the electron channel (right). Simulated signal and background contributions are scaled to the best fit results.

using a “blind” analysis with the optimisation based exclusively on regions where the signal contribution is negligible and all the selections frozen before the signal region has been looked at. It further provides an increase of the measurement sensitivity and a reduction of systematic uncertainties. The BDT analysis was designed following Ref. [29].

The adopted BDT algorithm constructs 400 decision trees using the Adaptive Boosting algorithm as implemented in Ref. [30]. The BDT training is carried out separately for the electron and muon final states, for each of the single-top-quark “2-jets 1-btag” and “3-jets 1-btag” signal-enriched regions, to provide a total of four BDTs. The background processes are input to the training according to their theoretical cross section predictions as outlined in Section 5. One third of the simulated signal and background samples are used for the training, one third are used to verify the performance of the trained BDT, while the remaining simulated data provide an unbiased sample used for the cross section evaluation.

Eleven observables reconstructed in the detector are chosen based on their power to discriminate between signal and background events.

The adopted variables are the lepton transverse momentum; the pseudorapidities of the most forward non-b-tagged jet and of the jet with the highest transverse momentum; the invariant mass of all reconstructed jets in the event; the angular separation between the two leading jets; the sums of the hadronic energy and of the hadronic transverse energy; the reconstructed top-quark mass using the jet with the highest b-tag discriminator; the reconstructed top-quark mass using the jet giving the reconstructed top-quark mass closest to $172 \text{ GeV}/c^2$; the cosine of the angle between the reconstructed W boson, in the rest frame of the sum of four-vectors of the W boson and leading jet, and the sum of four-vectors of the W boson and leading jet; and the sphericity of the event. The validity of the description of these input variables and the output of the BDT classifiers is confirmed in data with negligible signal contribution using a Kolmogorov–Smirnov test.

The QCD multijet background evaluation is described in Section 5. The determination of the single-top-quark production cross section in the t -channel, including the treatment of statistical and systematic uncertainties, is performed by using the classifier distributions in all 12 analysis categories simultaneously.

The measured distributions of the classifier outputs in the “2-jets 1-btag” and “3-jets 1-btag” signal enriched categories are shown separately for the muon and electron channel in Figs. 8 and 9. The measured distributions of the classifier outputs in the “2-jets 2-btags”, “3-jets 2-btags”, “4-jets 1-btag”, and “4-jets 2-btags” signal depleted categories are shown separately for the muon and electron channels in Fig. 10.

9 Determination of the Cross Section with Multivariate Analyses

The NN and BDT analyses employ a Bayesian approach [31] to measure the single-top-quark production cross section. The signal cross section is determined simultaneously from the data distributions of the corresponding multivariate discriminator, modelled as 1-dimensional histograms, in the different categories. The distributions for signal and backgrounds are taken from simulation, except for the QCD multijet distribution, which is derived from data. The signal yield is measured in terms of the signal strength μ which is defined as the actual cross section divided by the SM prediction. The probability to observe a certain dataset $p(\text{data}|\mu)$ is related to the posterior distribution $p(\mu|\text{data})$ of μ by using Bayes’ theorem

$$p(\mu|\text{data}) \propto p(\text{data}|\mu) \cdot \pi(\mu)$$

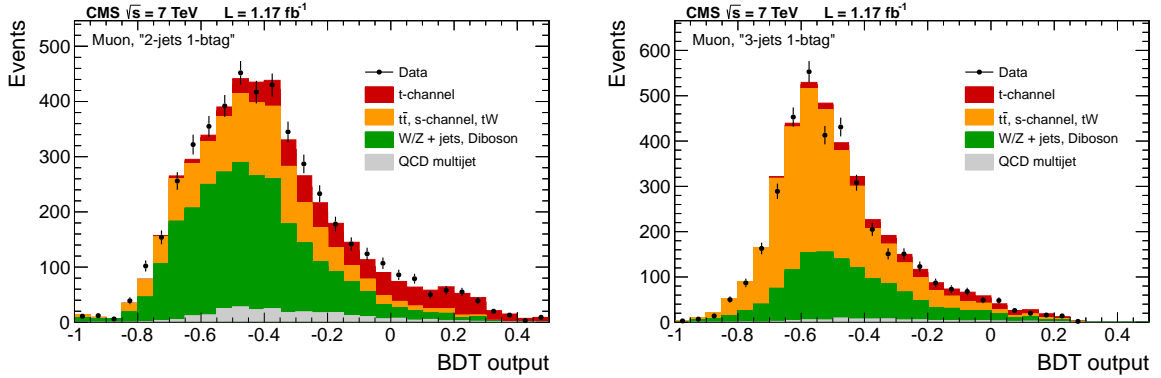


Figure 8: Distributions of the BDT discriminator output in the muon channel for the “2-jets 1-btag” (left) and “3-jets 1-btag” (right) categories. Simulated signal and background contributions are scaled to the best fit results.

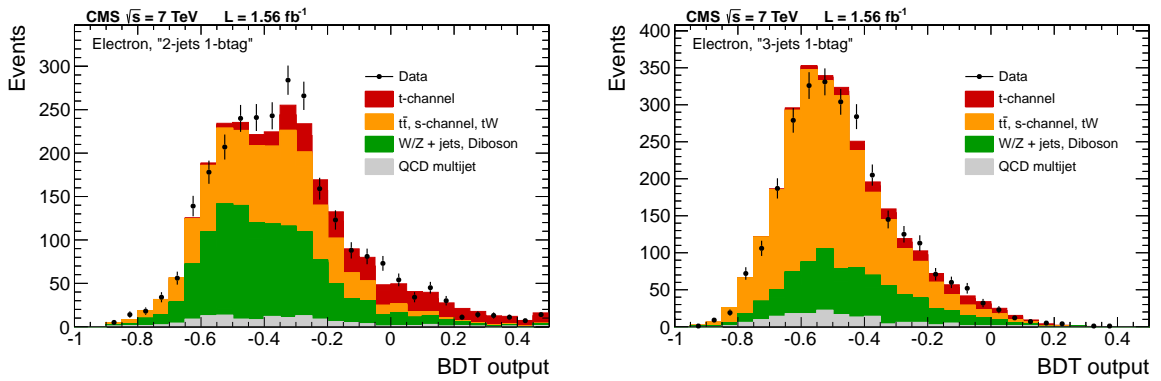


Figure 9: Distributions of the BDT discriminator output in the electron channel for the “2-jets 1-btag” (left) and “3-jets 1-btag” (right) categories. Simulated signal and background contributions are scaled to the best fit results.

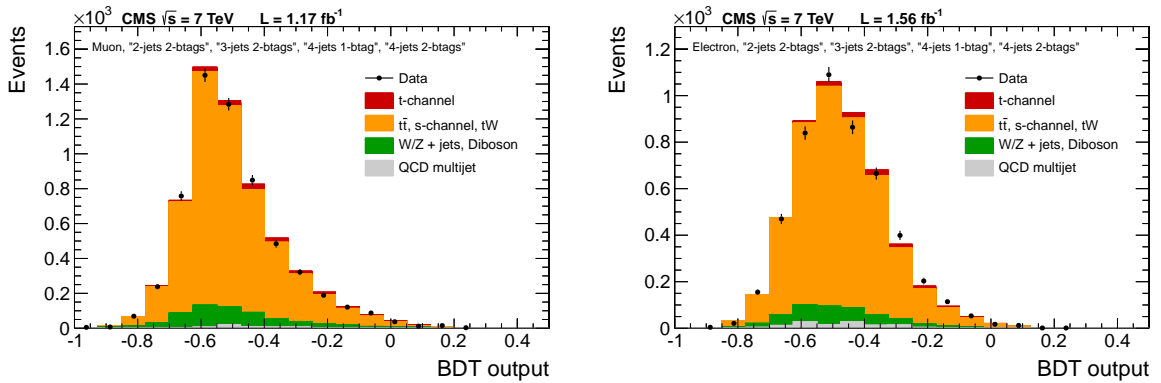


Figure 10: Distributions of the BDT discriminator output in the signal depleted categories for the muon channel (left) and electron channel (right). Simulated signal and background contributions are scaled to the best fit results.

where $\pi(\mu)$ denotes a uniform prior distribution of the signal strength.

Experimental uncertainties and cross-section uncertainties are included by introducing additional parameters $\vec{\theta}$ in the statistical model, extending the probability to observe a certain dataset to $p'(\text{data}|\mu, \vec{\theta})$, which depends on the nuisance parameters $\vec{\theta}$. This approach allows the nuisance parameter values to be constrained by data, thus reducing the respective uncertainties.

The m systematic uncertainties are included via nuisance parameters $\vec{\theta} = (\theta_1, \dots, \theta_m)$, which contain k normalisation parameters and $m - k$ parameters influencing the shape of the simulated distributions. For normalisation uncertainties $i = 1, \dots, k$, the priors $\pi_i(\theta_i)$ are log-normal distributions. The medians are set to the corresponding cross sections and the widths to their uncertainties. The priors for shape uncertainties are normal distributions. For each shape uncertainty, two shifted simulated discriminator distributions are derived, varying the corresponding uncertainty by $\pm 1\sigma$. Here, the parameter θ_i is used to interpolate between the nominal and shifted histograms.

The posterior distribution for the signal strength μ , $p(\mu|\text{data})$, is obtained by integrating the $(m + 1)$ -dimensional posterior in all nuisance parameters $\vec{\theta}$:

$$p(\mu|\text{data}) \propto \int p'(\text{data}|\mu, \vec{\theta}) \cdot \pi(\mu) \pi(\vec{\theta}) d\vec{\theta}.$$

This integration, also called *marginalisation*, is performed using the Markov chain MC method as implemented in the package THETA [32]. The central value is extracted from this distribution and used as μ . The central 68% quantile is taken as the total marginalised uncertainty in the measurement. It includes the statistical uncertainty and the m systematic uncertainties.

An estimate of the statistical uncertainty is taken from the total marginalised uncertainty after subtracting, in quadrature, the individual contributions of marginalised uncertainties. To obtain the individual contribution of each systematic uncertainty, the signal extraction procedure is repeated with signal and background contributions changed according to the systematic uncertainty. The mean shift of the cross section estimate, with respect to the value obtained in the nominal scenario, is taken as the corresponding impact on the signal cross section measurement.

However, modelling the systematic uncertainties as nuisance parameters requires an assumption for the dependence of p' on θ_i . This dependence is often unknown for theoretical uncertainties, in particular if they have an effect on the shape of the discriminator distribution. Therefore, such uncertainties are not included via additional nuisance parameters. Instead, their effect on the cross section measurement is estimated by performing pseudo-experiments as explained above, and their impact is added in quadrature to the total marginalised uncertainty.

In conclusion, systematic uncertainties are included with two different methods. Experimental uncertainties and cross-section uncertainties are included as additional parameters in the statistical model and marginalised. Theoretical uncertainties are not included as additional parameters in the statistical model, but their impact is added in quadrature to the total marginalised uncertainty.

10 Systematic Uncertainties and Measurement Sensitivity

For the $|\eta_{\gamma}|$ analysis, each systematic uncertainty is evaluated by generating pseudo-experiments, which take into account the effect of the corresponding systematic source on the distribution

of $|\eta_j|$ and on the event yield of the physics processes. Pseudo-experiments are generated separately with templates varied by $\pm 1\sigma$ of the corresponding uncertainty. A fit to $|\eta_j|$ is then performed on each pseudo-experiment. The mean shift of the fit results, with respect to the value obtained in the nominal scenario, is taken as the corresponding uncertainty.

In the BDT and NN analyses the experimental systematic uncertainties (excluding the luminosity) are marginalised with the Bayesian method. Theoretical uncertainties, however, are not marginalised, but are estimated by generating pseudo-experiments using separate templates, varied by $\pm 1\sigma$ for the corresponding uncertainty, for each source of systematic uncertainties, and repeating the signal extraction procedure.

A particular uncertainty, which is only present for the $|\eta_j|$ analysis, concerns the extraction of W+jets from data. It is evaluated by generating pseudo-experiments in the SB and repeating the signal extraction procedure and fit to $|\eta_j|$. This method exploits the ansatz that the distribution of $|\eta_j|$ is the same in both the SR and SB. The uncertainty is taken as the root mean square of the distribution of fit results obtained in this way. This uncertainty depends on the amount of available data in the SB and is uncorrelated between the muons and electron samples. In addition, alternative $|\eta_j|$ shapes are derived in the simulation by varying the Wb+X and Wc+X fractions of the background by factors of $\pm 30\%$ independently in the SR and SB regions. The fit procedure is repeated using the new shapes and the maximum difference in the result with respect to the central value is added in quadrature to the other uncertainties.

The following sources of systematic uncertainties are considered in all three analyses. Differences in the $|\eta_j|$ and the two multivariate analyses are remarked upon where relevant:

- **Jet energy scale (JES).** All reconstructed jet four-momenta in simulated events are simultaneously varied according to the η and p_T -dependent uncertainties on the jet energy scale [33]. This variation in jet four-momenta is also propagated to \cancel{E}_T . For multivariate analyses, the complete parameterisation of JES as in [33] is considered and all parameters are considered as nuisance parameters and included in the marginalisation procedure described in Section 9.
- **Jet energy resolution.** A smearing is applied to account for the known difference in jet energy resolution with respect to data [34], increasing or decreasing the extra resolution contribution by the uncertainty on the resolution.
- **b tagging.** Both b tagging and misidentification efficiencies in the data are estimated from control samples [20]. Scale factors are applied to simulated samples to reproduce the measured efficiencies. The corresponding uncertainties are propagated as systematic uncertainties. For multivariate analyses, b tagging average scale factors are constrained using the marginalisation procedure described in Section 9. The effect of any remaining, unconstrained, b tagging modelling is determined by modelling possible variations of the b tagging scale factors as a function of p_T and $|\eta|$, using different degrees (from one to five) of Chebyshev polynomials. The largest observed variation with respect to the nominal result is taken as the systematic uncertainty, and is found to be negligible.
- **Trigger.** Single lepton trigger efficiencies are estimated with a “tag and probe” method [35] from Drell–Yan data. The efficiencies of triggers requiring a lepton plus a b-tagged jet are parameterised as a function of the jet p_T and the value of the TCHP b-tag discriminator. The selection efficiencies have been validated using a reference trigger. The uncertainties of the parameterisation and an additional flavour dependency is propagated to the final result.

- **Pileup.** The effect of multiple interactions (pileup) is evaluated by reweighting simulated samples to reproduce the expected number of pileup interactions in data, properly taking into account in-time and out-of-time pileup contributions. The uncertainty on the expected number of pileup interactions (5%) is propagated as a systematic uncertainty to this measurement.
- **Missing transverse energy.** The \cancel{E}_T modelling uncertainty is propagated to the cross section measurement. The effect on \cancel{E}_T measurement of unclustered energy deposits in the calorimeters is included.
- **Luminosity.** The luminosity is known with a relative uncertainty of $\pm 2.2\%$ [36].
- **Background normalisation.** The uncertainties on the normalisation of each background source are listed below. They are propagated as systematic uncertainties in the $|\eta_j|$ analysis only for dibosons and s - and tW -channel single-top-quark processes. The remaining backgrounds are estimated from data. The uncertainty on $t\bar{t}$ is used as a Gaussian constraint in the signal-extraction fit. In the multivariate analyses, normalisation uncertainties are accounted for as a prior probability density function for the Bayesian inference using a log-normal model.
 - $t\bar{t}$: $\pm 15\%$, based on the statistical uncertainties in Ref. [37].
 - Dibosons, single-top-quark s - and tW -channels: $\pm 30\%$, $\pm 15\%$, $\pm 13\%$, respectively, based on theoretical uncertainties.
 - W/Z +jets: $\pm 100\%$, $\pm 50\%$, and $\pm 30\%$ are taken for $W+b/c$ flavour jets, W +light flavour jets, and Z +jets, respectively, consistent with previous estimates [37]. In the multivariate analyses, the various W +jets processes are considered to be uncorrelated, as are the different jet categories, in order to avoid too many model assumptions.
 - QCD multijet: the normalisation and the corresponding uncertainty is determined from data (see Section 5).
- **Limited MC data.** The uncertainty due to the limited amount of MC data in the templates used for the statistical inferences is determined by using the Barlow–Beeston method [38, 39].
- **Scale uncertainty.** The uncertainties on the renormalisation and factorisation scales are studied with dedicated single-top-quark and background samples of W +jets, Z +jets, and $t\bar{t}$ events. They are generated by doubling or halving the renormalisation and factorisation scale with respect to the nominal value equal to the Q^2 in the hard-scattering process.
- **Extra parton modelling (matching).** The uncertainty due to extra hard parton radiation is studied by doubling or halving the threshold for the MLM jet matching scheme [40] for W +jets, Z +jets, and $t\bar{t}$ from its default.
- **Signal generator.** The results obtained by using the nominal POWHEG signal samples are compared with the result obtained using signal samples generated by COMPHEP. In general, the largest model deviations occur in the kinematic distributions of the spectator b quark [41]. The differences in the transverse momentum distribution of the spectator b quark, at the generator level, between 4-flavour and 5-flavour scheme (FS) POWHEG [42] are more than a factor two smaller than the differences between POWHEG-5FS and COMPHEP over the whole p_T range. Pseudo-experiments with simulated COMPHEP events are generated and the nominal signal extraction procedure with POWHEG-5FS templates is repeated. Half of the observed shift of the cross section measurement is taken as the systematic uncertainty due to

Table 2: Sources of uncertainty on the cross section measurement.

		Uncertainty source	NN	BDT	$ \eta_{j'} $
Marginalised (NN, BDT)	Experimental uncert.	Statistical	-6.1/+5.5%	-4.7/+5.4%	$\pm 8.5\%$
		Limited MC data	-1.7/+2.3%	$\pm 3.1\%$	$\pm 0.9\%$
		Jet energy scale	-0.3/+1.9%	$\pm 0.6\%$	-3.9/+4.1%
		Jet energy resolution	-0.3/+0.6%	$\pm 0.1\%$	-0.7/+1.2%
		b tagging	-2.7/+3.1%	$\pm 1.6\%$	$\pm 3.1\%$
		Muon trigger + reco.	-2.2/+2.3%	$\pm 1.9\%$	-1.5/+1.7%
		Electron trigger + reco.	-0.6/+0.7%	$\pm 1.2\%$	-0.8/+0.9%
		Hadronic trigger	-1.3/+1.2%	$\pm 1.5\%$	$\pm 3.0\%$
		Pileup	-1.0/+0.9%	$\pm 0.4\%$	-0.3/+0.2%
	E_T modelling	-0.0/+0.2%	$\pm 0.2\%$	$\pm 0.5\%$	
	Backg. rates	W+jets	-2.0/+3.0%	-3.5/+2.5%	$\pm 5.9\%$
		light flavour (u, d, s, g)	-0.2/+0.3%	$\pm 0.4\%$	n/a
		heavy flavour (b, c)	-1.9/+2.9%	-3.5/+2.5%	n/a
		$t\bar{t}$	-0.9/+0.8%	$\pm 1.0\%$	$\pm 3.3\%$
		QCD, muon	$\pm 0.8\%$	$\pm 1.7\%$	$\pm 0.9\%$
QCD, electron		$\pm 0.4\%$	$\pm 0.8\%$	-0.4/+0.3%	
s-, tW ch., dibosons, Z+jets		$\pm 0.3\%$	$\pm 0.6\%$	$\pm 0.5\%$	
Total marginalised uncertainty		-7.7/+7.9%	-7.7/+7.8%	n/a	
Not marginalised	Luminosity			$\pm 2.2\%$	
	Theor. uncert.	Scale, $t\bar{t}$	-3.3/+1.0%	$\pm 0.9\%$	-4.0/+2.1%
		Scale, W+jets	-2.8/+0.3%	-0.0/+3.4%	n/a
		Scale, t-, s-, tW channels	-0.4/+1.0%	$\pm 0.2\%$	-2.2/+2.3%
		Matching, $t\bar{t}$	$\pm 1.3\%$	$\pm 0.4\%$	$\pm 0.4\%$
		t-channel generator	$\pm 4.2\%$	$\pm 4.6\%$	$\pm 2.5\%$
		PDF	$\pm 1.3\%$	$\pm 1.3\%$	$\pm 2.5\%$
		Total theor. uncertainty		-6.3/+4.8%	-4.9/+5.9%
Syst. + theor. + luminosity uncert.		-8.1/+7.8%	-8.1/+8.4%	$\pm 10.8\%$	
Total (stat. + syst. + theor. + lum.)		-10.1/+9.5%	-9.4/+10.0%	$\pm 13.8\%$	

signal generator modelling.

- **Parton distribution functions.** The uncertainty due to the choice of the parton distribution functions (PDF) is estimated using pseudo-experiments, reweighting the simulated events with each of the 40 eigenvectors of the CTEQ6 [18] PDF set and the central set of CTEQ10 [43], and repeating the nominal signal extraction procedure. For reweighting the simulated events, the LHAPDF [44] package is used.

The jet energy scale and jet energy resolution are fully correlated across all samples. The matching and scale uncertainties are fully correlated between W+jets and Z+jets, but are uncorrelated with $t\bar{t}$.

Table 2 summarises the different contributions to the systematic uncertainty on the combined (muon and electron) cross section measurement in the three analyses. For the multivariate analyses, experimental uncertainties and background rates are constrained from the marginalisation procedure (except for the luminosity), as described in Section 9. The remaining theoretical and luminosity uncertainties are added separately in quadrature to the total uncertainty.

11 Results

11.1 Individual analyses

The $|\eta_j|$ analysis yields the following cross section measurements for the muon and electron channels:

$$\begin{aligned}\sigma_{t\text{-ch.}} &= 73.3 \pm 10.4 \text{ (stat. + syst. + lum.)} \pm 4.0 \text{ (theor.) pb} \quad (\text{muons}), \\ \sigma_{t\text{-ch.}} &= 61.6 \pm 13.9 \text{ (stat. + syst. + lum.)} \pm 3.5 \text{ (theor.) pb} \quad (\text{electrons}).\end{aligned}$$

The two measurements are compatible, taking into account correlated and uncorrelated uncertainties. The uncorrelated uncertainties include the W +jets and QCD extraction procedure, lepton reconstruction and trigger efficiencies, and the hadronic part of the trigger.

Combining the muon and electron measurements gives

$$\sigma_{t\text{-ch.}} = 70.0 \pm 6.0 \text{ (stat.)} \pm 6.5 \text{ (syst.)} \pm 3.6 \text{ (theor.)} \pm 1.5 \text{ (lum.) pb.}$$

The Bayesian inference is performed with the data samples and the 50% quantile is calculated as the best parameter estimate for the signal strength μ . The 84% and 16% quantiles are quoted as upper and lower boundaries for the 1σ credible interval.

The measured single-top-quark t -channel production cross section in the NN analysis is

$$\begin{aligned}\sigma_{t\text{-ch.}} &= 69.7_{-7.0}^{+7.2} \text{ (stat. + syst. + lum.)} \pm 3.6 \text{ (theor.) pb} \quad (\text{muons}), \\ \sigma_{t\text{-ch.}} &= 65.1_{-8.9}^{+9.2} \text{ (stat. + syst. + lum.)} \pm 3.5 \text{ (theor.) pb} \quad (\text{electrons}).\end{aligned}$$

The quoted errors are the total uncertainties including marginalised, unmarginalised, and luminosity uncertainties. The two measurements are compatible within the uncertainties, after properly taking into account the correlated contributions. The combination of the muon and electron measurements gives

$$\sigma_{t\text{-ch.}} = 68.1 \pm 4.1 \text{ (stat.)} \pm 3.4 \text{ (syst.)}_{-4.3}^{+3.3} \text{ (theor.)} \pm 1.5 \text{ (lum.) pb.}$$

The measured single-top-quark t -channel production cross section in the BDT analysis is

$$\begin{aligned}\sigma_{t\text{-ch.}} &= 66.6_{-6.6}^{+7.0} \text{ (stat. + syst. + lum.)}_{-3.5}^{+6.4} \text{ (theor.) pb} \quad (\text{muons}), \\ \sigma_{t\text{-ch.}} &= 66.4_{-7.9}^{+8.4} \text{ (stat. + syst. + lum.)}_{-5.4}^{+5.4} \text{ (theor.) pb} \quad (\text{electrons}),\end{aligned}$$

and their combination gives

$$\sigma_{t\text{-ch.}} = 66.6 \pm 4.0 \text{ (stat.)} \pm 3.3 \text{ (syst.)}_{-3.3}^{+3.9} \text{ (theor.)} \pm 1.5 \text{ (lum.) pb.}$$

The results of the three analyses are consistent with the SM prediction.

11.2 Combination

The results of the three analyses are combined using the BLUE method. The statistical correlation between each pair of measurements is estimated by generating dedicated pseudo-experiments. The correlation is 60% between NN and $|\eta_{j'}|$, 69% between BDT and $|\eta_{j'}|$, and 74% between NN and BDT. Correlations for the jet energy scale and resolution, b tagging, and E_T modelling between $|\eta_{j'}|$ and the two multivariate analyses are expected to be small. This is because the determination of the corresponding nuisance parameters, from the marginalisation adopted in the BDT and NN analyses, is dominated by in-situ constraints from data samples independent of those used to determine uncertainties in the $|\eta_{j'}|$ analysis. The assumed correlation for those uncertainties is taken to be 20%. The correlation has, nevertheless, been varied from 0% to 50%, with a corresponding variation of the central value by -0.03 pb, and no appreciable variation has been observed for the combined uncertainty. For trigger uncertainties, the correlation between $|\eta_{j'}|$ and the two multivariate analyses is more difficult to ascertain. Varying the correlations in the combination from 0% to 100% results in a variation of the central value of 0.03 pb, with no appreciable variation of the combined uncertainty. All other uncertainties are determined mostly from the same data samples used by the two analyses, hence 100% correlation is assumed.

The BLUE method is applied iteratively, as previously carried out in Ref. [4]. In each iteration, the absolute uncertainty is calculated by scaling the relative uncertainties given in Table 2 with the combined value from the previous iteration. This is repeated until the combined value remains constant. There are no appreciable changes with respect to the non-iterative BLUE method. The 0.03 pb variation in the central value, due to changes in correlation coefficients, is added in quadrature to the total uncertainty. However, this results in a negligible additional contribution.

The χ^2 obtained by the BLUE combination of the three analyses is 0.19, corresponding to a p -value of 0.90. The results of the individual analyses are consistent with each other.

The combined result of the measured single-top-quark t -channel production cross section at $\sqrt{s} = 7$ TeV is

$$\sigma_{t\text{-ch.}} = 67.2 \pm 6.1 \text{ pb} = 67.2 \pm 3.7 \text{ (stat.)} \pm 3.0 \text{ (syst.)} \pm 3.5 \text{ (theor.)} \pm 1.5 \text{ (lum.) pb}$$

for an assumed top-quark mass of $172.5 \text{ GeV}/c^2$.

11.3 $|V_{tb}|$ Extraction

The absolute value of the CKM element $|V_{tb}|$ is determined in a similar fashion to Ref. [4], assuming that $|V_{td}|$ and $|V_{ts}|$ are much smaller than $|V_{tb}|$, as $|V_{tb}| = \sqrt{\sigma_{t\text{-ch.}}/\sigma_{t\text{-ch.}}^{\text{th.}}}$, where $\sigma_{t\text{-ch.}}^{\text{th.}}$ is the SM prediction calculated assuming $|V_{tb}| = 1$ [7]. If we take into account the possible presence of an anomalous Wtb coupling, this relation modifies taking into account an anomalous form factor f_{L_V} [45–47], which is not necessarily equal to 1 in beyond-the-SM models. We determine

$$|f_{L_V} V_{tb}| = \sqrt{\frac{\sigma_{t\text{-ch.}}}{\sigma_{t\text{-ch.}}^{\text{th.}}}} = 1.020 \pm 0.046 \text{ (meas.)} \pm 0.017 \text{ (theor.)},$$

where the first uncertainty term contains all uncertainties of the cross section measurement including theoretical ones, and the second is the uncertainty on the SM theoretical prediction. From this result, the confidence interval for $|V_{tb}|$, assuming the constraint $|V_{tb}| \leq 1$ and $f_{L_V} = 1$, is determined using the unified approach of Feldman and Cousins [48] to be

$$0.92 < |V_{tb}| \leq 1, \quad \text{at the 95\% confidence level.}$$

12 Conclusions

The cross section of t -channel single-top-quark production has been measured in pp collisions using 2011 data in semileptonic top-quark decay modes with improved precision compared to the previous CMS measurement. Two approaches have been adopted. One approach has been based on a fit of the characteristic pseudorapidity distribution of the light quark recoiling against the single top quark in the t -channel with background determination from data. The other has been based on two multivariate discriminators, a Neural Network and Boosted Decision Trees. The multivariate analyses reduce the impact of systematic uncertainties by simultaneously analysing phase space regions with substantial t -channel single-top-quark contributions, and regions where they are negligible. The results are all consistent within uncertainties. As a consequence, all three analyses have been combined with the Best Linear Unbiased Estimator method to obtain the final result.

The combined measurement of the single-top-quark t -channel cross section is 67.2 ± 6.1 pb. This is the first measurement with a relative uncertainty below 10%. It is in agreement with the approximate NNLO standard model prediction of $64.6^{+2.1+1.5}_{-0.7-1.7}$ pb [7]. Figure 11 compares this measurement with dedicated t -channel cross section measurements at the Tevatron [49, 50], ATLAS [5], and with the QCD expectations computed at NLO with MCFM in the 5-flavour scheme [51] and at approximate NNLO [7]. The absolute value of the CKM matrix element V_{tb} is measured to be $|f_{L_V} V_{tb}| = \sqrt{\sigma_{t\text{-ch.}} / \sigma_{t\text{-ch.}}^{\text{th.}}} = 1.020 \pm 0.046$ (meas.) ± 0.017 (theor.). Assuming $f_{L_V} = 1$ and $|V_{tb}| \leq 1$, we measure the 95% confidence level interval $0.92 < |V_{tb}| \leq 1$.

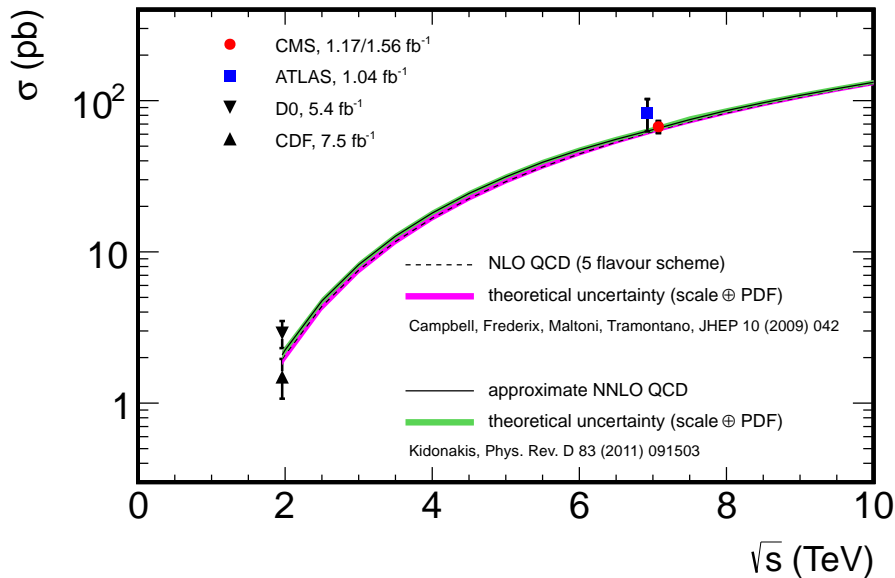


Figure 11: The single-top-quark cross section in the t -channel vs. centre-of-mass energy. The error band (width of the curve) of the SM calculation is obtained by varying the top-quark mass within its current uncertainty [3], estimating the PDF uncertainty according to HEPDATA recommendations [52], and varying the factorisation and renormalisation scales coherently by a factor of two up and down. The central values of the two SM predictions differ by 2.2% at $\sqrt{s} = 7$ TeV.

Acknowledgements

We congratulate our colleagues in the CERN accelerator departments for the excellent performance of the LHC machine. We thank the technical and administrative staff at CERN and other CMS institutes, and acknowledge support from BMWF and FWF (Austria); FNRS and FWO (Belgium); CNPq, CAPES, FAPERJ, and FAPESP (Brazil); MES (Bulgaria); CERN; CAS, MoST, and NSFC (China); COLCIENCIAS (Colombia); MSES (Croatia); RPF (Cyprus); MEYS (Czech Republic); MoER, SF0690030s09 and ERDF (Estonia); Academy of Finland, MEC, and HIP (Finland); CEA and CNRS/IN2P3 (France); BMBF, DFG, and HGF (Germany); GSRT (Greece); OTKA and NKTH (Hungary); DAE and DST (India); IPM (Iran); SFI (Ireland); INFN (Italy); NRF and WCU (Korea); LAS (Lithuania); CINVESTAV, CONACYT, SEP, and UASLP-FAI (Mexico); MSI (New Zealand); PAEC (Pakistan); MSHE and NSC (Poland); FCT (Portugal); JINR (Armenia, Belarus, Georgia, Ukraine, Uzbekistan); MON, RosAtom, RAS and RFBR (Russia); MSTD (Serbia); SEIDI and CPAN (Spain); Swiss Funding Agencies (Switzerland); NSC (Taipei); TUBITAK and TAEK (Turkey); NASU (Ukraine); STFC (United Kingdom); DOE and NSF (USA).

Individuals have received support from the Marie-Curie programme and the European Research Council (European Union); the Leventis Foundation; the A. P. Sloan Foundation; the Alexander von Humboldt Foundation; the Austrian Science Fund (FWF); the Belgian Federal Science Policy Office; the Fonds pour la Formation à la Recherche dans l'Industrie et dans l'Agriculture (FRIA-Belgium); the Agentschap voor Innovatie door Wetenschap en Technologie (IWT-Belgium); the Council of Science and Industrial Research, India; the Compagnia di San Paolo (Torino); and the HOMING PLUS programme of Foundation for Polish Science, co-financed from European Union, Regional Development Fund.

References

- [1] CDF Collaboration, "Observation of single top quark production and measurement of $|V_{tb}|$ with CDF", *Phys. Rev. D* **82** (2010) 112005, doi:10.1103/PhysRevD.82.112005, arXiv:1004.1181.
- [2] D0 Collaboration, "Measurements of single top quark production cross sections and $|V_{tb}|$ in $p\bar{p}$ collisions at $\sqrt{s} = 1.96$ TeV", *Phys. Rev. D* **84** (2011) 112001, doi:10.1103/PhysRevD.84.112001, arXiv:1108.3091.
- [3] CDF and D0 Collaborations, "Combination of CDF and D0 measurements of the single top production cross section", (2009). arXiv:0908.2171.
- [4] CMS Collaboration, "Measurement of the t -channel single top quark production cross section in pp collisions at $\sqrt{s} = 7$ TeV", *Phys. Rev. Lett.* **107** (2011) 091802, doi:10.1103/PhysRevLett.107.091802, arXiv:1106.3052.
- [5] ATLAS Collaboration, "Measurement of the t -channel single top-quark production cross section in pp collisions at $\sqrt{s} = 7$ TeV with the ATLAS detector", *Phys. Lett. B* **717** (2012) 330, doi:10.1016/j.physletb.2012.09.031, arXiv:1205.3130.
- [6] ATLAS Collaboration, "Evidence for the associated production of a W boson and a top quark in ATLAS at $\sqrt{s} = 7$ TeV", *Phys. Lett. B* **716** (2012) 142, doi:10.1016/j.physletb.2012.08.011, arXiv:1205.5764.

- [7] N. Kidonakis, “Next-to-next-to-leading-order collinear and soft gluon corrections for t-channel single top quark production”, *Phys. Rev. D* **83** (2011) 091503, doi:10.1103/PhysRevD.83.091503, arXiv:1103.2792.
- [8] L. Lyons, D. Gibaut, and P. Clifford, “How to combine correlated estimates of a single physical quantity”, *Nucl. Instr. and Meth. A* **270** (1988) 110, doi:10.1016/0168-9002(88)90018-6.
- [9] CMS Collaboration, “The CMS experiment at the CERN LHC”, *JINST* **03** (2008) S08004, doi:10.1088/1748-0221/3/08/S08004.
- [10] E. Re, “Single-top Wt-channel production matched with parton showers using the POWHEG method”, *Eur. Phys. J. C* **71** (2011) 1547, doi:10.1140/epjc/s10052-011-1547-z, arXiv:1009.2450.
- [11] S. Alioli et al., “A general framework for implementing NLO calculations in shower Monte Carlo programs: the POWHEG BOX”, *JHEP* **06** (2010) 043, doi:10.1007/JHEP06(2010)043, arXiv:1002.2581.
- [12] S. Alioli et al., “NLO single-top production matched with shower in POWHEG: s- and t-channel contributions”, *JHEP* **09** (2009) 111, doi:10.1088/1126-6708/2009/09/111, arXiv:0907.4076.
- [13] S. Frixione, P. Nason, and C. Oleari, “Matching NLO QCD computations with parton shower simulations: the POWHEG method”, *JHEP* **11** (2007) 070, doi:10.1088/1126-6708/2007/11/070, arXiv:0709.2092.
- [14] T. Sjöstrand, S. Mrenna, and P. Z. Skands, “PYTHIA 6.4 physics and manual”, *JHEP* **05** (2006) 026, doi:10.1088/1126-6708/2006/05/026, arXiv:hep-ph/0603175.
- [15] E. E. Boos et al., “CompHEP - computer system for calculation of particle collisions at high energies”, Preprint 89-63/140, Moscow State University, Institute for Nuclear Physics, (1989).
- [16] J. Alwall et al., “MadGraph 5: going beyond”, *JHEP* **06** (2011) 128, doi:10.1007/JHEP06(2011)128, arXiv:1106.0522.
- [17] J. Alwall et al., “Comparative study of various algorithms for the merging of parton showers and matrix elements in hadronic collisions”, *Eur. Phys. J. C* **53** (2008) 473, doi:10.1140/epjc/s10052-007-0490-5, arXiv:0706.2569.
- [18] J. Pumplin et al., “New generation of parton distributions with uncertainties from global QCD analysis”, *JHEP* **07** (2002) 012, doi:10.1088/1126-6708/2002/07/012, arXiv:hep-ph/0201195.
- [19] S. Agostinelli et al., “Geant4—a simulation toolkit”, *Nucl. Instrum. Meth. A* **506** (2003) 250, doi:10.1016/S0168-9002(03)01368-8.
- [20] CMS Collaboration, “b-Jet Identification in the CMS Experiment”, CMS Physics Analysis Summary CMS-PAS-BTV-11-004, (2011).
- [21] CMS Collaboration, “Measurement of the charge asymmetry in top-quark pair production in proton-proton collisions at $\sqrt{s} = 7$ TeV”, *Phys. Lett. B* **709** (2012) 28, doi:10.1016/j.physletb.2012.01.078, arXiv:1112.5100.

- [22] CMS Collaboration, “Particle–Flow Event Reconstruction in CMS and Performance for Jets, Taus, and E_T ”, CMS Physics Analysis Summary CMS-PAS-PFT-09-001, (2009).
- [23] M. Cacciari, G. P. Salam, and G. Soyez, “The anti- k_r jet clustering algorithm”, *JHEP* **04** (2008) 063, doi:10.1088/1126-6708/2008/04/063, arXiv:0802.1189.
- [24] ATLAS Collaboration, “Measurement of the cross section for the production of a W boson in association with b-jets in pp collisions at $\sqrt{s} = 7$ TeV with the ATLAS detector”, *Phys. Lett. B* **707** (2012) 418, doi:10.1016/j.physletb.2011.12.046, arXiv:1109.1470.
- [25] P. Motylinski, “Angular correlations in t-channel single top production at the LHC”, *Phys. Rev. D* **80** (2009) 074015, doi:10.1103/PhysRevD.80.074015, arXiv:0905.4754.
- [26] M. Feindt, “A neural bayesian estimator for conditional probability densities”, (2004). arXiv:physics/0402093.
- [27] M. Feindt and U. Kerzel, “The NeuroBayes neural network package”, *Nucl. Instrum. Meth. A* **559** (2006) 190, doi:10.1016/j.nima.2005.11.166.
- [28] B. Efron and R. J. Tibshirani, “An Introduction to the Bootstrap”. Chapman & Hall, New York, 1993.
- [29] H.-P. Bretz et al., “A development environment for visual physics analysis”, *JINST* **07** (2012) T08005, doi:10.1088/1748-0221/7/08/T08005, arXiv:1205.4912.
- [30] A. Hoecker et al., “TMVA: Toolkit for Multivariate Data Analysis”, (2007). arXiv:physics/0703039.
- [31] E. T. Jaynes, “Probability Theory: The Logic of Science”. Cambridge University Press, Cambridge, 2003.
- [32] T. Müller, J. Ott, and J. Wagner-Kuhr, “THETA – a framework for template-based statistical modeling and inference”, Preprint CMS/2012-1, (2012).
- [33] CMS Collaboration, “Determination of jet energy calibration and transverse momentum resolution in CMS”, *JINST* **06** (2011) 11002, doi:10.1088/1748-0221/6/11/P11002, arXiv:1107.4277.
- [34] CMS Collaboration, “Jet Energy Resolution in CMS at $\sqrt{s} = 7$ TeV”, CMS Physics Analysis Summary CMS-PAS-JME-10-014, (2010).
- [35] CMS Collaboration, “Measurements of inclusive W and Z cross sections in pp collisions at $\sqrt{s} = 7$ TeV”, *JHEP* **01** (2011) 080, doi:10.1007/JHEP01(2011)080, arXiv:1012.2466.
- [36] CMS Collaboration, “Absolute Calibration of the Luminosity Measurement at CMS: Winter 2012 Update”, CMS Physics Analysis Summary CMS-PAS-SMP-12-008, (2012).
- [37] CMS Collaboration, “Measurement of the $t\bar{t}$ production cross section in pp collisions at 7 TeV in lepton + jets events using b-quark jet identification”, *Phys. Rev. D* **84** (2011) 092004, doi:10.1103/PhysRevD.84.092004, arXiv:1108.3773.
- [38] R. J. Barlow and C. Beeston, “Fitting using finite Monte Carlo samples”, *Comput. Phys. Commun.* **77** (1993) 219, doi:10.1016/0010-4655(93)90005-w.

- [39] J. S. Conway, "Nuisance parameters in likelihoods for multisource spectra", in *Proceedings of PHYSTAT 2011 Workshop on Statistical Issues Related to Discovery Claims in Search Experiments and Unfolding*, H. B. Prosper and L. Lyons, eds., p. 115. CERN, 2011. arXiv:1103.0354.
- [40] M. L. Mangano et al., "Matching matrix elements and shower evolution for top-quark production in hadronic collisions", *JHEP* **01** (2007) 013, doi:10.1088/1126-6708/2007/01/013, arXiv:hep-ph/0611129.
- [41] J. M. Campbell et al., "Next-to-leading-order predictions for t-channel single-top production at hadron colliders", *Phys. Rev. Lett.* **102** (2009) 182003, doi:10.1103/PhysRevLett.102.182003, arXiv:0903.0005.
- [42] R. Frederix, E. Re, and P. Torrielli, "Single-top t-channel hadroproduction in the four-flavour scheme with POWHEG and aMC@NLO", (2012). arXiv:1207.5391.
- [43] H.-L. Lai et al., "New parton distributions for collider physics", *Phys. Rev. D* **82** (2010) 074024, doi:10.1103/PhysRevD.82.074024, arXiv:1007.2241.
- [44] M. R. Whalley, D. Bourilkov, and R. C. Group, "The Les Houches accord PDFs (LHAPDF) and LHAGLUE", (2005). arXiv:hep-ph/0508110.
- [45] J. A. Aguilar-Saavedra, "A minimal set of top anomalous couplings", *Nucl. Phys. B* **812** (2009) 181, doi:10.1016/j.nuclphysb.2008.12.012, arXiv:0811.3842.
- [46] G. L. Kane, G. A. Ladinsky, and C. P. Yuan, "Using the top quark for testing standard model polarization and CP predictions", *Phys. Rev. D* **45** (1992) 124, doi:10.1103/PhysRevD.45.124.
- [47] T. G. Rizzo, "Single top quark production as a probe for anomalous moments at hadron colliders", *Phys. Rev. D* **53** (1996) 6218, doi:10.1103/PhysRevD.53.6218, arXiv:hep-ph/9506351.
- [48] G. J. Feldman and R. D. Cousins, "A unified approach to the classical statistical analysis of small signals", *Phys. Rev. D* **57** (1998) 3873, doi:10.1103/PhysRevD.57.3873, arXiv:physics/9711021.
- [49] D0 Collaboration, "Model-independent measurement of t-channel single top quark production in $p\bar{p}$ collisions at $\sqrt{s} = 1.96$ TeV", *Phys. Lett. B* **705** (2011) 313, doi:10.1016/j.physletb.2011.10.035, arXiv:1105.2788.
- [50] CDF Collaboration, "First observation of electroweak single top quark production", *Phys. Rev. Lett.* **103** (2009) 092002, doi:10.1103/PhysRevLett.103.092002, arXiv:0903.0885.
- [51] J. M. Campbell et al., "NLO predictions for t-channel production of single top and fourth generation quarks at hadron colliders", *JHEP* **10** (2009) 042, doi:10.1088/1126-6708/2009/10/042, arXiv:0907.3933.
- [52] J. M. Campbell, J. W. Huston, and W. J. Stirling, "Hard interactions of quarks and gluons: A primer for LHC physics", *Rept. Prog. Phys.* **70** (2007) 89, doi:10.1088/0034-4885/70/1/R02, arXiv:hep-ph/0611148.

A The CMS Collaboration

Yerevan Physics Institute, Yerevan, Armenia

S. Chatrchyan, V. Khachatryan, A.M. Sirunyan, A. Tumasyan

Institut für Hochenergiephysik der OeAW, Wien, Austria

W. Adam, E. Aguilo, T. Bergauer, M. Dragicevic, J. Erö, C. Fabjan¹, M. Friedl, R. Frühwirth¹, V.M. Ghete, N. Hörmann, J. Hrubec, M. Jeitler¹, W. Kiesenhofer, V. Knünz, M. Krammer¹, I. Krätschmer, D. Liko, I. Mikulec, M. Pernicka[†], D. Rabady², B. Rahbaran, C. Rohringer, H. Rohringer, R. Schöfbeck, J. Strauss, A. Taurok, W. Waltenberger, C.-E. Wulz¹

National Centre for Particle and High Energy Physics, Minsk, Belarus

V. Mossolov, N. Shumeiko, J. Suarez Gonzalez

Universiteit Antwerpen, Antwerpen, Belgium

M. Bansal, S. Bansal, T. Cornelis, E.A. De Wolf, X. Janssen, S. Luyckx, L. Mucibello, S. Ochesanu, B. Roland, R. Rougny, M. Selvaggi, H. Van Haevermaet, P. Van Mechelen, N. Van Remortel, A. Van Spilbeeck

Vrije Universiteit Brussel, Brussel, Belgium

F. Blekman, S. Blyweert, J. D'Hondt, R. Gonzalez Suarez, A. Kalogeropoulos, M. Maes, A. Olbrechts, W. Van Doninck, P. Van Mulders, G.P. Van Onsem, I. Villella

Université Libre de Bruxelles, Bruxelles, Belgium

B. Clerbaux, G. De Lentdecker, V. Dero, A.P.R. Gay, T. Hreus, A. Léonard, P.E. Marage, A. Mohammadi, T. Reis, L. Thomas, C. Vander Velde, P. Vanlaer, J. Wang

Ghent University, Ghent, Belgium

V. Adler, K. Bernaert, A. Cimmino, S. Costantini, G. Garcia, M. Grunewald, B. Klein, J. Lellouch, A. Marinov, J. McCartin, A.A. Ocampo Rios, D. Ryckbosch, N. Strobbe, F. Thyssen, M. Tytgat, S. Walsh, E. Yazgan, N. Zaganidis

Université Catholique de Louvain, Louvain-la-Neuve, Belgium

S. Basegmez, G. Bruno, R. Castello, L. Ceard, C. Delaere, T. du Pree, D. Favart, L. Forthomme, A. Giammanco³, J. Hollar, V. Lemaitre, J. Liao, O. Militaru, C. Nuttens, D. Pagano, A. Pin, K. Piotrkowski, J.M. Vizan Garcia

Université de Mons, Mons, Belgium

N. Belyi, T. Caebergs, E. Daubie, G.H. Hammad

Centro Brasileiro de Pesquisas Fisicas, Rio de Janeiro, Brazil

G.A. Alves, M. Correa Martins Junior, T. Martins, M.E. Pol, M.H.G. Souza

Universidade do Estado do Rio de Janeiro, Rio de Janeiro, Brazil

W.L. Aldá Júnior, W. Carvalho, A. Custódio, E.M. Da Costa, D. De Jesus Damiao, C. De Oliveira Martins, S. Fonseca De Souza, H. Malbouisson, M. Malek, D. Matos Figueiredo, L. Mundim, H. Nogima, W.L. Prado Da Silva, A. Santoro, L. Soares Jorge, A. Sznajder, A. Vilela Pereira

Instituto de Fisica Teorica, Universidade Estadual Paulista, Sao Paulo, Brazil

T.S. Anjos⁴, C.A. Bernardes⁴, F.A. Dias⁵, T.R. Fernandez Perez Tomei, E.M. Gregores⁴, C. Lagana, F. Marinho, P.G. Mercadante⁴, S.F. Novaes, Sandra S. Padula

Institute for Nuclear Research and Nuclear Energy, Sofia, Bulgaria

V. Genchev², P. Iaydjiev², S. Piperov, M. Rodozov, S. Stoykova, G. Sultanov, V. Tcholakov, R. Trayanov, M. Vutova

University of Sofia, Sofia, Bulgaria

A. Dimitrov, R. Hadjiiska, V. Kozhuharov, L. Litov, B. Pavlov, P. Petkov

Institute of High Energy Physics, Beijing, China

J.G. Bian, G.M. Chen, H.S. Chen, C.H. Jiang, D. Liang, S. Liang, X. Meng, J. Tao, J. Wang, X. Wang, Z. Wang, H. Xiao, M. Xu, J. Zang, Z. Zhang

State Key Lab. of Nucl. Phys. and Tech., Peking University, Beijing, China

C. Asawatangtrakuldee, Y. Ban, Y. Guo, W. Li, S. Liu, Y. Mao, S.J. Qian, H. Teng, D. Wang, L. Zhang, W. Zou

Universidad de Los Andes, Bogota, Colombia

C. Avila, J.P. Gomez, B. Gomez Moreno, A.F. Osorio Oliveros, J.C. Sanabria

Technical University of Split, Split, Croatia

N. Godinovic, D. Lelas, R. Plestina⁶, D. Polic, I. Puljak²

University of Split, Split, Croatia

Z. Antunovic, M. Kovac

Institute Rudjer Boskovic, Zagreb, Croatia

V. Brigljevic, S. Duric, K. Kadija, J. Luetic, D. Mekterovic, S. Morovic

University of Cyprus, Nicosia, Cyprus

A. Attikis, M. Galanti, G. Mavromanolakis, J. Mousa, C. Nicolaou, F. Ptochos, P.A. Razis

Charles University, Prague, Czech Republic

M. Finger, M. Finger Jr.

Academy of Scientific Research and Technology of the Arab Republic of Egypt, Egyptian Network of High Energy Physics, Cairo, Egypt

Y. Assran⁷, N. Bakhet, S. Elgammal⁸, A. Ellithi Kamel⁹, S. Khalil⁸, A.M. Kuotb Awad¹⁰, M.A. Mahmoud¹⁰, A. Radi^{11,12}

National Institute of Chemical Physics and Biophysics, Tallinn, Estonia

M. Kadastik, M. Müntel, M. Raidal, L. Rebane, A. Tiko

Department of Physics, University of Helsinki, Helsinki, Finland

P. Eerola, G. Fedi, M. Voutilainen

Helsinki Institute of Physics, Helsinki, Finland

J. Härkönen, A. Heikkinen, V. Karimäki, R. Kinnunen, M.J. Kortelainen, T. Lampén, K. Lassila-Perini, S. Lehti, T. Lindén, P. Luukka, T. Mäenpää, T. Peltola, E. Tuominen, J. Tuominiemi, E. Tuovinen, D. Ungaro, L. Wendland

Lappeenranta University of Technology, Lappeenranta, Finland

K. Banzuzi, A. Karjalainen, A. Korpela, T. Tuuva

DSM/IRFU, CEA/Saclay, Gif-sur-Yvette, France

M. Besancon, S. Choudhury, M. Dejardin, D. Denegri, B. Fabbro, J.L. Faure, F. Ferri, S. Ganjour, A. Givernaud, P. Gras, G. Hamel de Monchenault, P. Jarry, E. Locci, J. Malcles, L. Millischer, A. Nayak, J. Rander, A. Rosowsky, M. Titov

Laboratoire Leprince-Ringuet, Ecole Polytechnique, IN2P3-CNRS, Palaiseau, France

S. Baffioni, F. Beaudette, L. Benhabib, L. Bianchini, M. Bluj¹³, P. Busson, C. Charlot, N. Daci, T. Dahms, M. Dalchenko, L. Dobrzynski, A. Florent, R. Granier de Cassagnac, M. Haguenaer,

P. Miné, C. Mironov, I.N. Naranjo, M. Nguyen, C. Ochando, P. Paganini, D. Sabes, R. Salerno, Y. Sirois, C. Veelken, A. Zabi

Institut Pluridisciplinaire Hubert Curien, Université de Strasbourg, Université de Haute Alsace Mulhouse, CNRS/IN2P3, Strasbourg, France

J.-L. Agram¹⁴, J. Andrea, D. Bloch, D. Bodin, J.-M. Brom, M. Cardaci, E.C. Chabert, C. Collard, E. Conte¹⁴, F. Drouhin¹⁴, J.-C. Fontaine¹⁴, D. Gelé, U. Goerlach, P. Juillot, A.-C. Le Bihan, P. Van Hove

Centre de Calcul de l'Institut National de Physique Nucleaire et de Physique des Particules, CNRS/IN2P3, Villeurbanne, France, Villeurbanne, France

F. Fassi, D. Mercier

Université de Lyon, Université Claude Bernard Lyon 1, CNRS-IN2P3, Institut de Physique Nucléaire de Lyon, Villeurbanne, France

S. Beauceron, N. Beaupere, O. Bondu, G. Boudoul, J. Chasserat, R. Chierici², D. Contardo, P. Depasse, H. El Mamouni, J. Fay, S. Gascon, M. Gouzevitch, B. Ille, T. Kurca, M. Lethuillier, L. Mirabito, S. Perries, L. Sgandurra, V. Sordini, Y. Tschudi, P. Verdier, S. Viret

E. Andronikashvili Institute of Physics, Academy of Science, Tbilisi, Georgia

V. Roinishvili

RWTH Aachen University, I. Physikalisches Institut, Aachen, Germany

C. Autermann, S. Beranek, B. Calpas, M. Edelhoff, L. Feld, N. Heracleous, O. Hindrichs, R. Jussen, K. Klein, J. Merz, A. Ostapchuk, A. Perieanu, F. Raupach, J. Sammet, S. Schael, D. Sprenger, H. Weber, B. Wittmer, V. Zhukov¹⁵

RWTH Aachen University, III. Physikalisches Institut A, Aachen, Germany

M. Ata, J. Caudron, E. Dietz-Laursonn, D. Duchardt, M. Erdmann, R. Fischer, A. Güth, T. Hebbeker, C. Heidemann, K. Hoepfner, D. Klingebiel, P. Kreuzer, M. Merschmeyer, A. Meyer, M. Olschewski, P. Papacz, H. Pieta, H. Reithler, S.A. Schmitz, L. Sonnenschein, J. Steggemann, D. Teysier, S. Thüer, M. Weber

RWTH Aachen University, III. Physikalisches Institut B, Aachen, Germany

M. Bontenackels, V. Cherepanov, Y. Erdogan, G. Flügge, H. Geenen, M. Geisler, W. Haj Ahmad, F. Hoehle, B. Kargoll, T. Kress, Y. Kuessel, J. Lingemann², A. Nowack, L. Perchalla, O. Pooth, P. Sauerland, A. Stahl

Deutsches Elektronen-Synchrotron, Hamburg, Germany

M. Aldaya Martin, J. Behr, W. Behrenhoff, U. Behrens, M. Bergholz¹⁶, A. Bethani, K. Borras, A. Burgmeier, A. Cakir, L. Calligaris, A. Campbell, E. Castro, F. Costanza, D. Dammann, C. Diez Pardos, G. Eckerlin, D. Eckstein, G. Flucke, A. Geiser, I. Glushkov, P. Gunnellini, S. Habib, J. Hauk, G. Hellwig, H. Jung, M. Kasemann, P. Katsas, C. Kleinwort, H. Kluge, A. Knutsson, M. Krämer, D. Krücker, E. Kuznetsova, W. Lange, J. Leonard, W. Lohmann¹⁶, B. Lutz, R. Mankel, I. Marfin, M. Marienfeld, I.-A. Melzer-Pellmann, A.B. Meyer, J. Mnich, A. Mussgiller, S. Naumann-Emme, O. Novgorodova, J. Olzem, H. Perrey, A. Petrukhin, D. Pitzl, A. Raspereza, P.M. Ribeiro Cipriano, C. Riedl, E. Ron, M. Rosin, J. Salfeld-Nebgen, R. Schmidt¹⁶, T. Schoerner-Sadenius, N. Sen, A. Spiridonov, M. Stein, R. Walsh, C. Wissing

University of Hamburg, Hamburg, Germany

V. Blobel, H. Enderle, J. Erfle, U. Gebbert, M. Görner, M. Gosselink, J. Haller, T. Hermanns, R.S. Höing, K. Kaschube, G. Kaussen, H. Kirschenmann, R. Klanner, J. Lange, F. Nowak, T. Peiffer, N. Pietsch, D. Rathjens, C. Sander, H. Schettler, P. Schleper, E. Schlieckau, A. Schmidt,

M. Schröder, T. Schum, M. Seidel, J. Sibille¹⁷, V. Sola, H. Stadie, G. Steinbrück, J. Thomsen, L. Vanelderren

Institut für Experimentelle Kernphysik, Karlsruhe, Germany

C. Barth, J. Berger, C. Böser, T. Chwalek, W. De Boer, A. Descroix, A. Dierlamm, M. Feindt, M. Guthoff², C. Hackstein, J. Hansen, F. Hartmann², T. Hauth², M. Heinrich, H. Held, K.H. Hoffmann, U. Husemann, I. Katkov¹⁵, J.R. Komaragiri, P. Lobelle Pardo, D. Martschei, S. Mueller, Th. Müller, M. Niegel, A. Nürnberg, O. Oberst, A. Oehler, J. Ott, G. Quast, K. Rabbertz, F. Ratnikov, N. Ratnikova, S. Röcker, F.-P. Schilling, G. Schott, H.J. Simonis, F.M. Stober, D. Troendle, R. Ulrich, J. Wagner-Kuhr, S. Wayand, T. Weiler, M. Zeise

Institute of Nuclear Physics "Demokritos", Aghia Paraskevi, Greece

G. Anagnostou, G. Daskalakis, T. Gerasis, S. Kesisoglou, A. Kyriakis, D. Loukas, I. Manolakas, A. Markou, C. Markou, E. Ntomari

University of Athens, Athens, Greece

L. Gouskos, T.J. Mertzimekis, A. Panagiotou, N. Saoulidou

University of Ioánnina, Ioánnina, Greece

I. Evangelou, C. Foudas, P. Kokkas, N. Manthos, I. Papadopoulos, V. Patras

KFKI Research Institute for Particle and Nuclear Physics, Budapest, Hungary

G. Bencze, C. Hajdu, P. Hidas, D. Horvath¹⁸, F. Sikler, V. Veszpremi, G. Vesztergombi¹⁹

Institute of Nuclear Research ATOMKI, Debrecen, Hungary

N. Beni, S. Czellar, J. Molnar, J. Palinkas, Z. Szillasi

University of Debrecen, Debrecen, Hungary

J. Karacsi, P. Raics, Z.L. Trocsanyi, B. Ujvari

Panjab University, Chandigarh, India

S.B. Beri, V. Bhatnagar, N. Dhingra, R. Gupta, M. Kaur, M.Z. Mehta, N. Nishu, L.K. Saini, A. Sharma, J.B. Singh

University of Delhi, Delhi, India

Ashok Kumar, Arun Kumar, S. Ahuja, A. Bhardwaj, B.C. Choudhary, S. Malhotra, M. Naimuddin, K. Ranjan, V. Sharma, R.K. Shivpuri

Saha Institute of Nuclear Physics, Kolkata, India

S. Banerjee, S. Bhattacharya, S. Dutta, B. Gomber, Sa. Jain, Sh. Jain, R. Khurana, S. Sarkar, M. Sharan

Bhabha Atomic Research Centre, Mumbai, India

A. Abdulsalam, D. Dutta, S. Kailas, V. Kumar, A.K. Mohanty², L.M. Pant, P. Shukla

Tata Institute of Fundamental Research - EHEP, Mumbai, India

T. Aziz, S. Ganguly, M. Guchait²⁰, A. Gurtu²¹, M. Maity²², G. Majumder, K. Mazumdar, G.B. Mohanty, B. Parida, K. Sudhakar, N. Wickramage

Tata Institute of Fundamental Research - HECR, Mumbai, India

S. Banerjee, S. Dugad

Institute for Research in Fundamental Sciences (IPM), Tehran, Iran

H. Arfaei²³, H. Bakhshiansohi, S.M. Etesami²⁴, A. Fahim²³, M. Hashemi²⁵, H. Hesari, A. Jafari, M. Khakzad, M. Mohammadi Najafabadi, S. Paktinat Mehdiabadi, B. Safarzadeh²⁶, M. Zeinali

INFN Sezione di Bari ^a, Università di Bari ^b, Politecnico di Bari ^c, Bari, Italy

M. Abbrescia^{a,b}, L. Barbone^{a,b}, C. Calabria^{a,b,2}, S.S. Chhibra^{a,b}, A. Colaleo^a, D. Creanza^{a,c}, N. De Filippis^{a,c,2}, M. De Palma^{a,b}, L. Fiore^a, G. Iaselli^{a,c}, G. Maggi^{a,c}, M. Maggi^a, B. Marangelli^{a,b}, S. My^{a,c}, S. Nuzzo^{a,b}, N. Pacifico^a, A. Pompili^{a,b}, G. Pugliese^{a,c}, G. Selvaggi^{a,b}, L. Silvestris^a, G. Singh^{a,b}, R. Venditti^{a,b}, P. Verwilligen^a, G. Zito^a

INFN Sezione di Bologna ^a, Università di Bologna ^b, Bologna, Italy

G. Abbiendi^a, A.C. Benvenuti^a, D. Bonacorsi^{a,b}, S. Braibant-Giacomelli^{a,b}, L. Brigliadori^{a,b}, P. Capiluppi^{a,b}, A. Castro^{a,b}, F.R. Cavallo^a, M. Cuffiani^{a,b}, G.M. Dallavalle^a, F. Fabbri^a, A. Fanfani^{a,b}, D. Fasanella^{a,b}, P. Giacomelli^a, C. Grandi^a, L. Guiducci^{a,b}, S. Marcellini^a, G. Masetti^a, M. Meneghelli^{a,b,2}, A. Montanari^a, F.L. Navarra^{a,b}, F. Odorici^a, A. Perrotta^a, F. Primavera^{a,b}, A.M. Rossi^{a,b}, T. Rovelli^{a,b}, G.P. Siroli^{a,b}, N. Tosi, R. Travaglini^{a,b}

INFN Sezione di Catania ^a, Università di Catania ^b, Catania, Italy

S. Albergo^{a,b}, G. Cappello^{a,b}, M. Chiorboli^{a,b}, S. Costa^{a,b}, R. Potenza^{a,b}, A. Tricomi^{a,b}, C. Tuve^{a,b}

INFN Sezione di Firenze ^a, Università di Firenze ^b, Firenze, Italy

G. Barbagli^a, V. Ciulli^{a,b}, C. Civinini^a, R. D'Alessandro^{a,b}, E. Focardi^{a,b}, S. Frosali^{a,b}, E. Gallo^a, S. Gonzi^{a,b}, M. Meschini^a, S. Paoletti^a, G. Sguazzoni^a, A. Tropiano^{a,b}

INFN Laboratori Nazionali di Frascati, Frascati, Italy

L. Benussi, S. Bianco, S. Colafranceschi²⁷, F. Fabbri, D. Piccolo

INFN Sezione di Genova ^a, Università di Genova ^b, Genova, Italy

P. Fabbriatore^a, R. Musenich^a, S. Tosi^{a,b}

INFN Sezione di Milano-Bicocca ^a, Università di Milano-Bicocca ^b, Milano, Italy

A. Benaglia^a, F. De Guio^{a,b}, L. Di Matteo^{a,b,2}, S. Fiorendi^{a,b}, S. Gennai^{a,2}, A. Ghezzi^{a,b}, S. Malvezzi^a, R.A. Manzoni^{a,b}, A. Martelli^{a,b}, A. Massironi^{a,b}, D. Menasce^a, L. Moroni^a, M. Paganoni^{a,b}, D. Pedrini^a, S. Ragazzi^{a,b}, N. Redaelli^a, S. Sala^a, T. Tabarelli de Fatis^{a,b}

INFN Sezione di Napoli ^a, Università di Napoli "Federico II" ^b, Napoli, Italy

S. Buontempo^a, C.A. Carrillo Montoya^a, N. Cavallo^{a,28}, A. De Cosa^{a,b,2}, O. Dogangun^{a,b}, F. Fabozzi^{a,28}, A.O.M. Iorio^{a,b}, L. Lista^a, S. Meola^{a,29}, M. Merola^a, P. Paolucci^{a,2}

INFN Sezione di Padova ^a, Università di Padova ^b, Università di Trento (Trento) ^c, Padova, Italy

P. Azzi^a, N. Bacchetta^{a,2}, P. Bellan^{a,b}, D. Bisello^{a,b}, A. Branca^{a,b,2}, R. Carlin^{a,b}, P. Checchia^a, T. Dorigo^a, U. Dosselli^a, F. Gasparini^{a,b}, U. Gasparini^{a,b}, A. Gozzelino^a, K. Kanishchev^{a,c}, S. Lacaprara^a, I. Lazzizzera^{a,c}, M. Margoni^{a,b}, A.T. Meneguzzo^{a,b}, M. Nespolo^{a,2}, J. Pazzini^{a,b}, P. Ronchese^{a,b}, F. Simonetto^{a,b}, E. Torassa^a, S. Vanini^{a,b}, P. Zotto^{a,b}, G. Zumerle^{a,b}

INFN Sezione di Pavia ^a, Università di Pavia ^b, Pavia, Italy

M. Gabusi^{a,b}, S.P. Ratti^{a,b}, C. Riccardi^{a,b}, P. Torre^{a,b}, P. Vitulo^{a,b}

INFN Sezione di Perugia ^a, Università di Perugia ^b, Perugia, Italy

M. Biasini^{a,b}, G.M. Bilei^a, L. Fanò^{a,b}, P. Lariccia^{a,b}, G. Mantovani^{a,b}, M. Menichelli^a, A. Nappi^{a,b,†}, F. Romeo^{a,b}, A. Saha^a, A. Santocchia^{a,b}, A. Spiezia^{a,b}, S. Taroni^{a,b}

INFN Sezione di Pisa ^a, Università di Pisa ^b, Scuola Normale Superiore di Pisa ^c, Pisa, Italy

P. Azzurri^{a,c}, G. Bagliesi^a, T. Boccali^a, G. Broccolo^{a,c}, R. Castaldi^a, R.T. D'Agnolo^{a,c,2}, R. Dell'Orso^a, F. Fiori^{a,b,2}, L. Foà^{a,c}, A. Giassi^a, A. Kraan^a, F. Ligabue^{a,c}, T. Lomtadze^a, L. Martini^{a,30}, A. Messineo^{a,b}, F. Palla^a, A. Rizzi^{a,b}, A.T. Serban^{a,31}, P. Spagnolo^a, P. Squillacioti^{a,2}, R. Tenchini^a, G. Tonelli^{a,b}, A. Venturi^a, P.G. Verdini^a

INFN Sezione di Roma ^a, Università di Roma ^b, Roma, Italy

L. Barone^{a,b}, F. Cavallari^a, D. Del Re^{a,b}, M. Diemoz^a, C. Fanelli^{a,b}, M. Grassi^{a,b,2}, E. Longo^{a,b}, P. Meridiani^{a,2}, F. Micheli^{a,b}, S. Nourbakhsh^{a,b}, G. Organtini^{a,b}, R. Paramatti^a, S. Rahatlou^{a,b}, M. Sigamani^a, L. Soffi^{a,b}

INFN Sezione di Torino ^a, Università di Torino ^b, Università del Piemonte Orientale (Novara) ^c, Torino, Italy

N. Amapane^{a,b}, R. Arcidiacono^{a,c}, S. Argiro^{a,b}, M. Arneodo^{a,c}, C. Biino^a, N. Cartiglia^a, S. Casasso^{a,b}, M. Costa^{a,b}, N. Demaria^a, C. Mariotti^{a,2}, S. Maselli^a, E. Migliore^{a,b}, V. Monaco^{a,b}, M. Musich^{a,2}, M.M. Obertino^{a,c}, N. Pastrone^a, M. Pelliccioni^a, A. Potenza^{a,b}, A. Romero^{a,b}, M. Ruspa^{a,c}, R. Sacchi^{a,b}, A. Solano^{a,b}, A. Staiano^a

INFN Sezione di Trieste ^a, Università di Trieste ^b, Trieste, Italy

S. Belforte^a, V. Candolise^{a,b}, M. Casarsa^a, F. Cossutti^a, G. Della Ricca^{a,b}, B. Gobbo^a, M. Marone^{a,b,2}, D. Montanino^{a,b,2}, A. Penzo^a, A. Schizzi^{a,b}

Kangwon National University, Chunchon, Korea

T.Y. Kim, S.K. Nam

Kyungpook National University, Daegu, Korea

S. Chang, D.H. Kim, G.N. Kim, D.J. Kong, H. Park, D.C. Son, T. Son

Chonnam National University, Institute for Universe and Elementary Particles, Kwangju, Korea

J.Y. Kim, Zero J. Kim, S. Song

Korea University, Seoul, Korea

S. Choi, D. Gyun, B. Hong, M. Jo, H. Kim, T.J. Kim, K.S. Lee, D.H. Moon, S.K. Park, Y. Roh

University of Seoul, Seoul, Korea

M. Choi, J.H. Kim, C. Park, I.C. Park, S. Park, G. Ryu

Sungkyunkwan University, Suwon, Korea

Y. Choi, Y.K. Choi, J. Goh, M.S. Kim, E. Kwon, B. Lee, J. Lee, S. Lee, H. Seo, I. Yu

Vilnius University, Vilnius, Lithuania

M.J. Bilinskas, I. Grigelionis, M. Janulis, A. Juodagalvis

Centro de Investigacion y de Estudios Avanzados del IPN, Mexico City, Mexico

H. Castilla-Valdez, E. De La Cruz-Burelo, I. Heredia-de La Cruz, R. Lopez-Fernandez, J. Martínez-Ortega, A. Sánchez-Hernández, L.M. Villasenor-Cendejas

Universidad Iberoamericana, Mexico City, Mexico

S. Carrillo Moreno, F. Vazquez Valencia

Benemerita Universidad Autonoma de Puebla, Puebla, Mexico

H.A. Salazar Ibarguen

Universidad Autónoma de San Luis Potosí, San Luis Potosí, Mexico

E. Casimiro Linares, A. Morelos Pineda, M.A. Reyes-Santos

University of Auckland, Auckland, New Zealand

D. Krofcheck

University of Canterbury, Christchurch, New Zealand

A.J. Bell, P.H. Butler, R. Doesburg, S. Reucroft, H. Silverwood

National Centre for Physics, Quaid-I-Azam University, Islamabad, Pakistan

M. Ahmad, M.I. Asghar, J. Butt, H.R. Hoorani, S. Khalid, W.A. Khan, T. Khurshid, S. Qazi, M.A. Shah, M. Shoaib

National Centre for Nuclear Research, Swierk, Poland

H. Bialkowska, B. Boimska, T. Frueboes, M. Górski, M. Kazana, K. Nawrocki, K. Romanowska-Rybinska, M. Szeleper, G. Wrochna, P. Zalewski

Institute of Experimental Physics, Faculty of Physics, University of Warsaw, Warsaw, Poland

G. Brona, K. Bunkowski, M. Cwiok, W. Dominik, K. Doroba, A. Kalinowski, M. Konecki, J. Krolikowski, M. Misiura

Laboratório de Instrumentação e Física Experimental de Partículas, Lisboa, Portugal

N. Almeida, P. Bargassa, A. David, P. Faccioli, P.G. Ferreira Parracho, M. Gallinaro, J. Seixas, J. Varela, P. Vischia

Joint Institute for Nuclear Research, Dubna, Russia

I. Belotelov, P. Bunin, M. Gavrilenko, I. Golutvin, I. Gorbunov, A. Kamenev, V. Karjavin, G. Kozlov, A. Lanev, A. Malakhov, P. Moisenz, V. Palichik, V. Perelygin, S. Shmatov, V. Smirnov, A. Volodko, A. Zarubin

Petersburg Nuclear Physics Institute, Gatchina (St. Petersburg), Russia

S. Evstyukhin, V. Golovtsov, Y. Ivanov, V. Kim, P. Levchenko, V. Murzin, V. Oreshkin, I. Smirnov, V. Sulimov, L. Uvarov, S. Vavilov, A. Vorobyev, An. Vorobyev

Institute for Nuclear Research, Moscow, Russia

Yu. Andreev, A. Dermenev, S. Gninenko, N. Golubev, M. Kirsanov, N. Krasnikov, V. Matveev, A. Pashenkov, D. Tlisov, A. Toropin

Institute for Theoretical and Experimental Physics, Moscow, Russia

V. Epshteyn, M. Erofeeva, V. Gavrilo, M. Kossov, N. Lychkovskaya, V. Popov, G. Safronov, S. Semenov, I. Shreyber, V. Stolin, E. Vlasov, A. Zhokin

Moscow State University, Moscow, Russia

A. Belyaev, E. Boos, M. Dubinin⁵, L. Dudko, A. Ershov, A. Gribushin, V. Klyukhin, O. Kodolova, I. Lokhtin, A. Markina, S. Obraztsov, M. Perfilov, S. Petrushanko, A. Popov, L. Sarycheva[†], V. Savrin, A. Snigirev

P.N. Lebedev Physical Institute, Moscow, Russia

V. Andreev, M. Azarkin, I. Dremin, M. Kirakosyan, A. Leonidov, G. Mesyats, S.V. Rusakov, A. Vinogradov

State Research Center of Russian Federation, Institute for High Energy Physics, Protvino, Russia

I. Azhgirey, I. Bayshev, S. Bitioukov, V. Grishin², V. Kachanov, D. Konstantinov, V. Krychkine, V. Petrov, R. Ryutin, A. Sobol, L. Tourtchanovitch, S. Troshin, N. Tyurin, A. Uzunian, A. Volkov

University of Belgrade, Faculty of Physics and Vinca Institute of Nuclear Sciences, Belgrade, Serbia

P. Adzic³², M. Djordjevic, M. Ekmedzic, D. Krpic³², J. Milosevic

Centro de Investigaciones Energéticas Medioambientales y Tecnológicas (CIEMAT), Madrid, Spain

M. Aguilar-Benitez, J. Alcaraz Maestre, P. Arce, C. Battilana, E. Calvo, M. Cerrada, M. Chamizo Llatas, N. Colino, B. De La Cruz, A. Delgado Peris, D. Domínguez Vázquez, C. Fernandez

Bedoya, J.P. Fernández Ramos, A. Ferrando, J. Flix, M.C. Fouz, P. Garcia-Abia, O. Gonzalez Lopez, S. Goy Lopez, J.M. Hernandez, M.I. Josa, G. Merino, J. Puerta Pelayo, A. Quintario Olmeda, I. Redondo, L. Romero, J. Santaolalla, M.S. Soares, C. Willmott

Universidad Autónoma de Madrid, Madrid, Spain

C. Albajar, G. Codispoti, J.F. de Trocóniz

Universidad de Oviedo, Oviedo, Spain

H. Brun, J. Cuevas, J. Fernandez Menendez, S. Folgueras, I. Gonzalez Caballero, L. Lloret Iglesias, J. Piedra Gomez

Instituto de Física de Cantabria (IFCA), CSIC-Universidad de Cantabria, Santander, Spain

J.A. Brochero Cifuentes, I.J. Cabrillo, A. Calderon, S.H. Chuang, J. Duarte Campderros, M. Felcini³³, M. Fernandez, G. Gomez, J. Gonzalez Sanchez, A. Graziano, C. Jorda, A. Lopez Virto, J. Marco, R. Marco, C. Martinez Rivero, F. Matorras, F.J. Munoz Sanchez, T. Rodrigo, A.Y. Rodríguez-Marrero, A. Ruiz-Jimeno, L. Scodellaro, I. Vila, R. Vilar Cortabitarte

CERN, European Organization for Nuclear Research, Geneva, Switzerland

D. Abbaneo, E. Auffray, G. Auzinger, M. Bachtis, P. Baillon, A.H. Ball, D. Barney, J.F. Benitez, C. Bernet⁶, G. Bianchi, P. Bloch, A. Bocci, A. Bonato, C. Botta, H. Breuker, T. Camporesi, G. Cerminara, T. Christiansen, J.A. Coarasa Perez, D. D'Enterria, A. Dabrowski, A. De Roeck, S. Di Guida, M. Dobson, N. Dupont-Sagorin, A. Elliott-Peisert, B. Frisch, W. Funk, G. Georgiou, M. Giffels, D. Gigi, K. Gill, D. Giordano, M. Girone, M. Giunta, F. Glege, R. Gomez-Reino Garrido, P. Govoni, S. Gowdy, R. Guida, S. Gundacker, J. Hammer, M. Hansen, P. Harris, C. Hartl, J. Harvey, B. Hegner, A. Hinzmann, V. Innocente, P. Janot, K. Kaadze, E. Karavakis, K. Kousouris, P. Lecoq, Y.-J. Lee, P. Lenzi, C. Lourenço, N. Magini, T. Mäki, M. Malberti, L. Malgeri, M. Mannelli, L. Masetti, F. Meijers, S. Mersi, E. Meschi, R. Moser, M.U. Mozer, M. Mulders, P. Musella, E. Nesvold, L. Orsini, E. Palencia Cortezon, E. Perez, L. Perrozzi, A. Petrilli, A. Pfeiffer, M. Pierini, M. Pimiä, D. Piparo, G. Polese, L. Quertenmont, A. Racz, W. Reece, J. Rodrigues Antunes, G. Rolandi³⁴, C. Rovelli³⁵, M. Rovere, H. Sakulin, F. Santanastasio, C. Schäfer, C. Schwick, I. Segoni, S. Sekmen, A. Sharma, P. Siegrist, P. Silva, M. Simon, P. Sphicas³⁶, D. Spiga, A. Tsirou, G.I. Veres¹⁹, J.R. Vlimant, H.K. Wöhri, S.D. Worm³⁷, W.D. Zeuner

Paul Scherrer Institut, Villigen, Switzerland

W. Bertl, K. Deiters, W. Erdmann, K. Gabathuler, R. Horisberger, Q. Ingram, H.C. Kaestli, S. König, D. Kotlinski, U. Langenegger, F. Meier, D. Renker, T. Rohe

Institute for Particle Physics, ETH Zurich, Zurich, Switzerland

L. Bäni, P. Bortignon, M.A. Buchmann, B. Casal, N. Chanon, A. Deisher, G. Dissertori, M. Dittmar, M. Donegà, M. Dünser, P. Eller, J. Eugster, K. Freudenreich, C. Grab, D. Hits, P. Lecomte, W. Lustermann, A.C. Marini, P. Martinez Ruiz del Arbol, N. Mohr, F. Moortgat, C. Nägeli³⁸, P. Nef, F. Nessi-Tedaldi, F. Pandolfi, L. Pape, F. Pauss, M. Peruzzi, F.J. Ronga, M. Rossini, L. Sala, A.K. Sanchez, A. Starodumov³⁹, B. Stieger, M. Takahashi, L. Tauscher[†], A. Thea, K. Theofilatos, D. Treille, C. Urscheler, R. Wallny, H.A. Weber, L. Wehrli

Universität Zürich, Zurich, Switzerland

C. AMSler⁴⁰, V. Chiochia, S. De Visscher, C. Favaro, M. Ivova Rikova, B. Kilminster, B. Millan Mejias, P. Otiougova, P. Robmann, H. Snoek, S. Tuppiti, M. Verzetti

National Central University, Chung-Li, Taiwan

Y.H. Chang, K.H. Chen, C. Ferro, C.M. Kuo, S.W. Li, W. Lin, Y.J. Lu, A.P. Singh, R. Volpe, S.S. Yu

National Taiwan University (NTU), Taipei, Taiwan

P. Bartalini, P. Chang, Y.H. Chang, Y.W. Chang, Y. Chao, K.F. Chen, C. Dietz, U. Grundler, W.-S. Hou, Y. Hsiung, K.Y. Kao, Y.J. Lei, R.-S. Lu, D. Majumder, E. Petrakou, X. Shi, J.G. Shiu, Y.M. Tzeng, X. Wan, M. Wang

Chulalongkorn University, Bangkok, Thailand

B. Asavapibhop, N. Srimanobhas

Cukurova University, Adana, Turkey

A. Adiguzel, M.N. Bakirci⁴¹, S. Cerci⁴², C. Dozen, I. Dumanoglu, E. Eskut, S. Girgis, G. Gokbulut, E. Gurpinar, I. Hos, E.E. Kangal, T. Karaman, G. Karapinar⁴³, A. Kayis Topaksu, G. Onengut, K. Ozdemir, S. Ozturk⁴⁴, A. Polatoz, K. Sogut⁴⁵, D. Sunar Cerci⁴², B. Tali⁴², H. Topakli⁴¹, L.N. Vergili, M. Vergili

Middle East Technical University, Physics Department, Ankara, Turkey

I.V. Akin, T. Aliev, B. Bilin, S. Bilmis, M. Deniz, H. Gamsizkan, A.M. Guler, K. Ocalan, A. Ozpineci, M. Serin, R. Sever, U.E. Surat, M. Yalvac, E. Yildirim, M. Zeyrek

Bogazici University, Istanbul, Turkey

E. Gülmez, B. Isildak⁴⁶, M. Kaya⁴⁷, O. Kaya⁴⁷, S. Ozkorucuklu⁴⁸, N. Sonmez⁴⁹

Istanbul Technical University, Istanbul, Turkey

K. Cankocak

National Scientific Center, Kharkov Institute of Physics and Technology, Kharkov, Ukraine

L. Levchuk

University of Bristol, Bristol, United Kingdom

J.J. Brooke, E. Clement, D. Cussans, H. Flacher, R. Frazier, J. Goldstein, M. Grimes, G.P. Heath, H.F. Heath, L. Kreczko, S. Metson, D.M. Newbold³⁷, K. Nirunpong, A. Poll, S. Senkin, V.J. Smith, T. Williams

Rutherford Appleton Laboratory, Didcot, United Kingdom

L. Basso⁵⁰, K.W. Bell, A. Belyaev⁵⁰, C. Brew, R.M. Brown, D.J.A. Cockerill, J.A. Coughlan, K. Harder, S. Harper, J. Jackson, B.W. Kennedy, E. Olaiya, D. Petyt, B.C. Radburn-Smith, C.H. Shepherd-Themistocleous, I.R. Tomalin, W.J. Womersley

Imperial College, London, United Kingdom

R. Bainbridge, G. Ball, R. Beuselinck, O. Buchmuller, D. Colling, N. Cripps, M. Cutajar, P. Dauncey, G. Davies, M. Della Negra, W. Ferguson, J. Fulcher, D. Futyan, A. Gilbert, A. Guneratne Bryer, G. Hall, Z. Hatherell, J. Hays, G. Iles, M. Jarvis, G. Karapostoli, L. Lyons, A.-M. Magnan, J. Marrouche, B. Mathias, R. Nandi, J. Nash, A. Nikitenko³⁹, J. Pela, M. Pesaresi, K. Petridis, M. Pioppi⁵¹, D.M. Raymond, S. Rogerson, A. Rose, M.J. Ryan, C. Seez, P. Sharp[†], A. Sparrow, M. Stoye, A. Tapper, M. Vazquez Acosta, T. Virdee, S. Wakefield, N. Wardle, T. Whyntie

Brunel University, Uxbridge, United Kingdom

M. Chadwick, J.E. Cole, P.R. Hobson, A. Khan, P. Kyberd, D. Leggat, D. Leslie, W. Martin, I.D. Reid, P. Symonds, L. Teodorescu, M. Turner

Baylor University, Waco, USA

K. Hatakeyama, H. Liu, T. Scarborough

The University of Alabama, Tuscaloosa, USA

O. Charaf, C. Henderson, P. Rumerio

Boston University, Boston, USA

A. Avetisyan, T. Bose, C. Fantasia, A. Heister, J. St. John, P. Lawson, D. Lazic, J. Rohlf, D. Sperka, L. Sulak

Brown University, Providence, USA

J. Alimena, S. Bhattacharya, G. Christopher, D. Cutts, Z. Demiragli, A. Ferapontov, A. Garabedian, U. Heintz, S. Jabeen, G. Kukartsev, E. Laird, G. Landsberg, M. Luk, M. Narain, D. Nguyen, M. Segala, T. Sinthuprasith, T. Speer

University of California, Davis, Davis, USA

R. Breedon, G. Breto, M. Calderon De La Barca Sanchez, S. Chauhan, M. Chertok, J. Conway, R. Conway, P.T. Cox, J. Dolen, R. Erbacher, M. Gardner, R. Houtz, W. Ko, A. Kopecky, R. Lander, O. Mall, T. Miceli, D. Pellett, F. Ricci-tam, B. Rutherford, M. Searle, J. Smith, M. Squires, M. Tripathi, R. Vasquez Sierra, R. Yohay

University of California, Los Angeles, Los Angeles, USA

V. Andreev, D. Cline, R. Cousins, J. Duris, S. Erhan, P. Everaerts, C. Farrell, J. Hauser, M. Ignatenko, C. Jarvis, G. Rakness, P. Schlein[†], P. Traczyk, V. Valuev, M. Weber

University of California, Riverside, Riverside, USA

J. Babb, R. Clare, M.E. Dinardo, J. Ellison, J.W. Gary, F. Giordano, G. Hanson, H. Liu, O.R. Long, A. Luthra, H. Nguyen, S. Paramesvaran, J. Sturdy, S. Sumowidagdo, R. Wilken, S. Wimpenny

University of California, San Diego, La Jolla, USA

W. Andrews, J.G. Branson, G.B. Cerati, S. Cittolin, D. Evans, A. Holzner, R. Kelley, M. Lebourgeois, J. Letts, I. Macneill, B. Mangano, S. Padhi, C. Palmer, G. Petrucciani, M. Pieri, M. Sani, V. Sharma, S. Simon, E. Sudano, M. Tadel, Y. Tu, A. Vartak, S. Wasserbaech⁵², F. Würthwein, A. Yagil, J. Yoo

University of California, Santa Barbara, Santa Barbara, USA

D. Barge, R. Bellan, C. Campagnari, M. D'Alfonso, T. Danielson, K. Flowers, P. Geffert, F. Golf, J. Incandela, C. Justus, P. Kalavase, D. Kovalskyi, V. Krutelyov, S. Lowette, R. Magaña Villalba, N. Mccoll, V. Pavlunin, J. Ribnik, J. Richman, R. Rossin, D. Stuart, W. To, C. West

California Institute of Technology, Pasadena, USA

A. Apresyan, A. Bornheim, Y. Chen, E. Di Marco, J. Duarte, M. Gataullin, Y. Ma, A. Mott, H.B. Newman, C. Rogan, M. Spiropulu, V. Timciuc, J. Veverka, R. Wilkinson, S. Xie, Y. Yang, R.Y. Zhu

Carnegie Mellon University, Pittsburgh, USA

V. Azzolini, A. Calamba, R. Carroll, T. Ferguson, Y. Iiyama, D.W. Jang, Y.F. Liu, M. Paulini, H. Vogel, I. Vorobiev

University of Colorado at Boulder, Boulder, USA

J.P. Cumalat, B.R. Drell, W.T. Ford, A. Gaz, E. Luiggi Lopez, J.G. Smith, K. Stenson, K.A. Ulmer, S.R. Wagner

Cornell University, Ithaca, USA

J. Alexander, A. Chatterjee, N. Eggert, L.K. Gibbons, B. Heltsley, W. Hopkins, A. Khukhunaishvili, B. Kreis, N. Mirman, G. Nicolas Kaufman, J.R. Patterson, A. Ryd, E. Salvati, W. Sun, W.D. Teo, J. Thom, J. Thompson, J. Tucker, J. Vaughan, Y. Weng, L. Winstrom, P. Wittich

Fairfield University, Fairfield, USA

D. Winn

Fermi National Accelerator Laboratory, Batavia, USA

S. Abdullin, M. Albrow, J. Anderson, L.A.T. Bauerdick, A. Beretvas, J. Berryhill, P.C. Bhat, K. Burkett, J.N. Butler, V. Chetluru, H.W.K. Cheung, F. Chlebana, V.D. Elvira, I. Fisk, J. Freeman, Y. Gao, D. Green, O. Gutsche, J. Hanlon, R.M. Harris, J. Hirschauer, B. Hooberman, S. Jindariani, M. Johnson, U. Joshi, B. Klima, S. Kunori, S. Kwan, C. Leonidopoulos⁵³, J. Linacre, D. Lincoln, R. Lipton, J. Lykken, K. Maeshima, J.M. Marraffino, S. Maruyama, D. Mason, P. McBride, K. Mishra, S. Mrenna, Y. Musienko⁵⁴, C. Newman-Holmes, V. O'Dell, O. Prokofyev, E. Sexton-Kennedy, S. Sharma, W.J. Spalding, L. Spiegel, L. Taylor, S. Tkaczyk, N.V. Tran, L. Uplegger, E.W. Vaandering, R. Vidal, J. Whitmore, W. Wu, F. Yang, J.C. Yun

University of Florida, Gainesville, USA

D. Acosta, P. Avery, D. Bourilkov, M. Chen, T. Cheng, S. Das, M. De Gruttola, G.P. Di Giovanni, D. Dobur, A. Drozdetskiy, R.D. Field, M. Fisher, Y. Fu, I.K. Furic, J. Gartner, J. Hugon, B. Kim, J. Konigsberg, A. Korytov, A. Kropivnitskaya, T. Kypreos, J.F. Low, K. Matchev, P. Milenovic⁵⁵, G. Mitselmakher, L. Muniz, M. Park, R. Remington, A. Rinkevicius, P. Sellers, N. Skhirtladze, M. Snowball, J. Yelton, M. Zakaria

Florida International University, Miami, USA

V. Gaultney, S. Hewamanage, L.M. Lebolo, S. Linn, P. Markowitz, G. Martinez, J.L. Rodriguez

Florida State University, Tallahassee, USA

T. Adams, A. Askew, J. Bochenek, J. Chen, B. Diamond, S.V. Gleyzer, J. Haas, S. Hagopian, V. Hagopian, M. Jenkins, K.F. Johnson, H. Prosper, V. Veeraraghavan, M. Weinberg

Florida Institute of Technology, Melbourne, USA

M.M. Baarmand, B. Dorney, M. Hohlmann, H. Kalakhety, I. Vodopyanov, F. Yumiceva

University of Illinois at Chicago (UIC), Chicago, USA

M.R. Adams, I.M. Anghel, L. Apanasevich, Y. Bai, V.E. Bazterra, R.R. Betts, I. Bucinskaite, J. Callner, R. Cavanaugh, O. Evdokimov, L. Gauthier, C.E. Gerber, D.J. Hofman, S. Khalatyan, F. Lacroix, C. O'Brien, C. Silkworth, D. Strom, P. Turner, N. Varelas

The University of Iowa, Iowa City, USA

U. Akgun, E.A. Albayrak, B. Bilki⁵⁶, W. Clarida, F. Duru, S. Griffiths, J.-P. Merlo, H. Mermerkaya⁵⁷, A. Mestvirishvili, A. Moeller, J. Nachtman, C.R. Newsom, E. Norbeck, Y. Onel, F. Ozok⁵⁸, S. Sen, P. Tan, E. Tiras, J. Wetzel, T. Yetkin, K. Yi

Johns Hopkins University, Baltimore, USA

B.A. Barnett, B. Blumenfeld, S. Bolognesi, D. Fehling, G. Giurgiu, A.V. Gritsan, Z.J. Guo, G. Hu, P. Maksimovic, M. Swartz, A. Whitbeck

The University of Kansas, Lawrence, USA

P. Baringer, A. Bean, G. Benelli, R.P. Kenny III, M. Murray, D. Noonan, S. Sanders, R. Stringer, G. Tinti, J.S. Wood

Kansas State University, Manhattan, USA

A.F. Barfuss, T. Bolton, I. Chakaberia, A. Ivanov, S. Khalil, M. Makouski, Y. Maravin, S. Shrestha, I. Svintradze

Lawrence Livermore National Laboratory, Livermore, USA

J. Gronberg, D. Lange, F. Rebassoo, D. Wright

University of Maryland, College Park, USA

A. Baden, B. Calvert, S.C. Eno, J.A. Gomez, N.J. Hadley, R.G. Kellogg, M. Kirn, T. Kolberg, Y. Lu, M. Marionneau, A.C. Mignerey, K. Pedro, A. Skuja, J. Temple, M.B. Tonjes, S.C. Tonwar

Massachusetts Institute of Technology, Cambridge, USA

A. Apyan, G. Bauer, J. Bendavid, W. Busza, E. Butz, I.A. Cali, M. Chan, V. Dutta, G. Gomez Ceballos, M. Goncharov, Y. Kim, M. Klute, K. Krajczar⁵⁹, A. Levin, P.D. Luckey, T. Ma, S. Nahn, C. Paus, D. Ralph, C. Roland, G. Roland, M. Rudolph, G.S.F. Stephans, F. Stöckli, K. Sumorok, K. Sung, D. Velicanu, E.A. Wenger, R. Wolf, B. Wyslouch, M. Yang, Y. Yilmaz, A.S. Yoon, M. Zanetti, V. Zhukova

University of Minnesota, Minneapolis, USA

S.I. Cooper, B. Dahmes, A. De Benedetti, G. Franzoni, A. Gude, S.C. Kao, K. Klapoetke, Y. Kubota, J. Mans, N. Pastika, R. Rusack, M. Sasseville, A. Singovsky, N. Tambe, J. Turkewitz

University of Mississippi, Oxford, USA

L.M. Cremaldi, R. Kroeger, L. Perera, R. Rahmat, D.A. Sanders

University of Nebraska-Lincoln, Lincoln, USA

E. Avdeeva, K. Bloom, S. Bose, D.R. Claes, A. Dominguez, M. Eads, J. Keller, I. Kravchenko, J. Lazo-Flores, S. Malik, G.R. Snow

State University of New York at Buffalo, Buffalo, USA

A. Godshalk, I. Iashvili, S. Jain, A. Kharchilava, A. Kumar, S. Rappoccio

Northeastern University, Boston, USA

G. Alverson, E. Barberis, D. Baumgartel, M. Chasco, J. Haley, D. Nash, T. Orimoto, D. Trocino, D. Wood, J. Zhang

Northwestern University, Evanston, USA

A. Anastassov, K.A. Hahn, A. Kubik, L. Lusito, N. Mucia, N. Odell, R.A. Ofierzynski, B. Pollack, A. Pozdnyakov, M. Schmitt, S. Stoynev, M. Velasco, S. Won

University of Notre Dame, Notre Dame, USA

L. Antonelli, D. Berry, A. Brinkerhoff, K.M. Chan, M. Hildreth, C. Jessop, D.J. Karmgard, J. Kolb, K. Lannon, W. Luo, S. Lynch, N. Marinelli, D.M. Morse, T. Pearson, M. Planer, R. Ruchti, J. Slaunwhite, N. Valls, M. Wayne, M. Wolf

The Ohio State University, Columbus, USA

B. Bylsma, L.S. Durkin, C. Hill, R. Hughes, K. Kotov, T.Y. Ling, D. Puigh, M. Rodenburg, C. Vuosalo, G. Williams, B.L. Winer

Princeton University, Princeton, USA

E. Berry, P. Elmer, V. Halyo, P. Hebda, J. Hegeman, A. Hunt, P. Jindal, S.A. Koay, D. Lopes Pegna, P. Lujan, D. Marlow, T. Medvedeva, M. Mooney, J. Olsen, P. Piroué, X. Quan, A. Raval, H. Saka, D. Stickland, C. Tully, J.S. Werner, A. Zuranski

University of Puerto Rico, Mayaguez, USA

E. Brownson, A. Lopez, H. Mendez, J.E. Ramirez Vargas

Purdue University, West Lafayette, USA

E. Alagoz, V.E. Barnes, D. Benedetti, G. Bolla, D. Bortoletto, M. De Mattia, A. Everett, Z. Hu, M. Jones, O. Koybasi, M. Kress, A.T. Laasanen, N. Leonardo, V. Maroussov, P. Merkel, D.H. Miller, N. Neumeister, I. Shipsey, D. Silvers, A. Svyatkovskiy, M. Vidal Marono, H.D. Yoo, J. Zablocki, Y. Zheng

Purdue University Calumet, Hammond, USA

S. Guragain, N. Parashar

Rice University, Houston, USA

A. Adair, B. Akgun, C. Boulahouache, K.M. Ecklund, F.J.M. Geurts, W. Li, B.P. Padley, R. Redjimi, J. Roberts, J. Zabel

University of Rochester, Rochester, USA

B. Betchart, A. Bodek, Y.S. Chung, R. Covarelli, P. de Barbaro, R. Demina, Y. Eshaq, T. Ferbel, A. Garcia-Bellido, P. Goldenzweig, J. Han, A. Harel, D.C. Miner, D. Vishnevskiy, M. Zielinski

The Rockefeller University, New York, USA

A. Bhatti, R. Ciesielski, L. Demortier, K. Goulios, G. Lungu, S. Malik, C. Mesropian

Rutgers, the State University of New Jersey, Piscataway, USA

S. Arora, A. Barker, J.P. Chou, C. Contreras-Campana, E. Contreras-Campana, D. Duggan, D. Ferencek, Y. Gershtein, R. Gray, E. Halkiadakis, D. Hidas, A. Lath, S. Panwalkar, M. Park, R. Patel, V. Rekovic, J. Robles, K. Rose, S. Salur, S. Schnetzer, C. Seitz, S. Somalwar, R. Stone, S. Thomas, M. Walker

University of Tennessee, Knoxville, USA

G. Cerizza, M. Hollingsworth, S. Spanier, Z.C. Yang, A. York

Texas A&M University, College Station, USA

R. Eusebi, W. Flanagan, J. Gilmore, T. Kamon⁶⁰, V. Khotilovich, R. Montalvo, I. Osipenkov, Y. Pakhotin, A. Perloff, J. Roe, A. Safonov, T. Sakuma, S. Sengupta, I. Suarez, A. Tatarinov, D. Toback

Texas Tech University, Lubbock, USA

N. Akchurin, J. Damgov, C. Dragoiu, P.R. Duderu, C. Jeong, K. Kovitanggoon, S.W. Lee, T. Libeiro, I. Volobouev

Vanderbilt University, Nashville, USA

E. Appelt, A.G. Delannoy, C. Florez, S. Greene, A. Gurrola, W. Johns, P. Kurt, C. Maguire, A. Melo, M. Sharma, P. Sheldon, B. Snook, S. Tuo, J. Velkovska

University of Virginia, Charlottesville, USA

M.W. Arenton, M. Balazs, S. Boutle, B. Cox, B. Francis, J. Goodell, R. Hirosky, A. Ledovskoy, C. Lin, C. Neu, J. Wood

Wayne State University, Detroit, USA

S. Gollapinni, R. Harr, P.E. Karchin, C. Kottachchi Kankanamge Don, P. Lamichhane, A. Sakharov

University of Wisconsin, Madison, USA

M. Anderson, D. Belknap, L. Borrello, D. Carlsmith, M. Cepeda, S. Dasu, E. Friis, L. Gray, K.S. Grogg, M. Grothe, R. Hall-Wilton, M. Herndon, A. Hervé, P. Klabbers, J. Klukas, A. Lanaro, C. Lazaridis, R. Loveless, A. Mohapatra, I. Ojalvo, F. Palmonari, G.A. Pierro, I. Ross, A. Savin, W.H. Smith, J. Swanson

†: Deceased

1: Also at Vienna University of Technology, Vienna, Austria

2: Also at CERN, European Organization for Nuclear Research, Geneva, Switzerland

3: Also at National Institute of Chemical Physics and Biophysics, Tallinn, Estonia

4: Also at Universidade Federal do ABC, Santo Andre, Brazil

5: Also at California Institute of Technology, Pasadena, USA

6: Also at Laboratoire Leprince-Ringuet, Ecole Polytechnique, IN2P3-CNRS, Palaiseau, France

7: Also at Suez Canal University, Suez, Egypt

- 8: Also at Zewail City of Science and Technology, Zewail, Egypt
- 9: Also at Cairo University, Cairo, Egypt
- 10: Also at Fayoum University, El-Fayoum, Egypt
- 11: Also at British University, Cairo, Egypt
- 12: Now at Ain Shams University, Cairo, Egypt
- 13: Also at National Centre for Nuclear Research, Swierk, Poland
- 14: Also at Université de Haute-Alsace, Mulhouse, France
- 15: Also at Moscow State University, Moscow, Russia
- 16: Also at Brandenburg University of Technology, Cottbus, Germany
- 17: Also at The University of Kansas, Lawrence, USA
- 18: Also at Institute of Nuclear Research ATOMKI, Debrecen, Hungary
- 19: Also at Eötvös Loránd University, Budapest, Hungary
- 20: Also at Tata Institute of Fundamental Research - HECR, Mumbai, India
- 21: Now at King Abdulaziz University, Jeddah, Saudi Arabia
- 22: Also at University of Visva-Bharati, Santiniketan, India
- 23: Also at Sharif University of Technology, Tehran, Iran
- 24: Also at Isfahan University of Technology, Isfahan, Iran
- 25: Also at Shiraz University, Shiraz, Iran
- 26: Also at Plasma Physics Research Center, Science and Research Branch, Islamic Azad University, Tehran, Iran
- 27: Also at Facoltà Ingegneria Università di Roma, Roma, Italy
- 28: Also at Università della Basilicata, Potenza, Italy
- 29: Also at Università degli Studi Guglielmo Marconi, Roma, Italy
- 30: Also at Università degli Studi di Siena, Siena, Italy
- 31: Also at University of Bucharest, Faculty of Physics, Bucuresti-Magurele, Romania
- 32: Also at Faculty of Physics of University of Belgrade, Belgrade, Serbia
- 33: Also at University of California, Los Angeles, Los Angeles, USA
- 34: Also at Scuola Normale e Sezione dell' INFN, Pisa, Italy
- 35: Also at INFN Sezione di Roma, Roma, Italy
- 36: Also at University of Athens, Athens, Greece
- 37: Also at Rutherford Appleton Laboratory, Didcot, United Kingdom
- 38: Also at Paul Scherrer Institut, Villigen, Switzerland
- 39: Also at Institute for Theoretical and Experimental Physics, Moscow, Russia
- 40: Also at Albert Einstein Center for Fundamental Physics, BERN, Switzerland
- 41: Also at Gaziosmanpasa University, Tokat, Turkey
- 42: Also at Adiyaman University, Adiyaman, Turkey
- 43: Also at Izmir Institute of Technology, Izmir, Turkey
- 44: Also at The University of Iowa, Iowa City, USA
- 45: Also at Mersin University, Mersin, Turkey
- 46: Also at Ozyegin University, Istanbul, Turkey
- 47: Also at Kafkas University, Kars, Turkey
- 48: Also at Suleyman Demirel University, Isparta, Turkey
- 49: Also at Ege University, Izmir, Turkey
- 50: Also at School of Physics and Astronomy, University of Southampton, Southampton, United Kingdom
- 51: Also at INFN Sezione di Perugia; Università di Perugia, Perugia, Italy
- 52: Also at Utah Valley University, Orem, USA
- 53: Now at University of Edinburgh, Scotland, Edinburgh, United Kingdom
- 54: Also at Institute for Nuclear Research, Moscow, Russia

55: Also at University of Belgrade, Faculty of Physics and Vinca Institute of Nuclear Sciences, Belgrade, Serbia

56: Also at Argonne National Laboratory, Argonne, USA

57: Also at Erzincan University, Erzincan, Turkey

58: Also at Mimar Sinan University, Istanbul, Istanbul, Turkey

59: Also at KFKI Research Institute for Particle and Nuclear Physics, Budapest, Hungary

60: Also at Kyungpook National University, Daegu, Korea